Inorganic Chemistry
Article

Inorg. Chem. **2009**, *48*, 9831–9845 **9831**
DOI: 10.1021/ic901393m

Spin Maximization from $S = 11$ to $S = 16$ in Mn_7 Disk-Like Clusters: Spin Frustration Effects and Their Computational Rationalization

Theocharis C. Stamatatos,[†] Dolos Foguet-Albiol,[†] Katye M. Poole,[‡] Wolfgang Wernsdorfer,[§] Khalil A. Abboud,[†] Ted A. O'Brien,[‡,∥] and George Christou*,[†]

[†]*Department of Chemistry, University of Florida, Gainesville, Florida 32611-7200,* [‡]*Department of Chemistry and Chemical Biology, Indiana University-Purdue University Indianapolis, Indianapolis, Indiana 46202-3274, and* [§]*Institut Néel, CNRS and Université J. Fournier, BP 166, 38042 Grenoble Cedex 9, France.*
[∥] *Deceased, March 2008.*

Received July 17, 2009

The use has been explored in Mn cluster chemistry of N_3^- or Cl^- in combination with *N*-methyldiethanolamine ($mdaH_2$) or triethanolamine ($teaH_3$). The reactions of $Mn(ClO_4)_2 \cdot 6H_2O$, NEt_3, NaN_3, and either $mdaH_2$ or $teaH_3$ (1:2:1:2) in DMF/MeOH afford $\{[Na(MeOH)_3][Mn_7(N_3)_6(mda)_6]\}_n$ (**1**) and $\{Na[Mn_7(N_3)_6(teaH)_6]\}_n$ (**2**), respectively, whereas the 2:1:1 reaction of $MnCl_2 \cdot 4H_2O$, $mdaH_2$, and NEt_3 in MeCN gives $(NHEt_3)[Mn_7Cl_6(mda)_6]$ (**3**). Similar reactions using $NBu^n_4N_3$ in place of NaN_3 gave $(NHEt_3)[Mn_7(N_3)_6(mda)_6]$ (**4**) and $(NHEt_3)[Mn_7(N_3)_6(teaH)_6]$ (**5**). The Mn_7 anions consist of a Mn_6 hexagon of alternating Mn^{II} and Mn^{III} ions surrounding a central Mn^{II} ion. The remaining ligation is by six bridging and chelating mda^{2-} or $teaH^{2-}$ groups, and either six terminal N_3^- (**1**, **2**, **4**, **5**) or Cl^- (**3**) ions. Each bridging mda^{2-} or $teaH^{2-}$ ligand contains both μ- and μ_3-O atoms, resulting in a similar, near-planar $[Mn_7(\mu_3\text{-}OR)_6(\mu\text{-}OR)_6]^{5+}$ core for all three complexes. The Mn_7 anions of **1** and **2** are connected via Na^+ cations to yield one-dimensional zigzag chains and three-dimensional windmill-like "hexagons-of-hexagons", respectively. In contrast, the Mn_7 anion of **3** forms a strong hydrogen-bond between the $NHEt_3^+$ cation and a terminal Cl^- ion giving a discrete ion-pair. Variable-temperature, solid-state direct current (dc) and alternating current (ac) magnetization studies were carried out in the 5.0−300 K range. Fits of dc magnetization versus field (H) and temperature (T) data by matrix diagonalization gave $S = 11$, $g = 1.95$, $D = -0.15$ cm^{-1} for **1**, $S = 16$, $g = 1.95$, $D = -0.02$ cm^{-1} for **2**, and $S = 11$, $g = 1.92$, $D = -0.13$ cm^{-1} for **3** (D is the axial zero-field splitting parameter). Complexes **4** and **5** were also found to possess $S = 11$ and $S = 16$ ground states, respectively. The different ground states of **1** and **2** were rationalized on the basis of the sign and magnitude of the various Mn_2 exchange parameters obtained from density functional theory (DFT) calculations. This analysis confirmed the presence of spin frustration effects, with the ground states being determined by the relative magnitude of the two weakest interactions. The combined results demonstrate the usefulness of *N*-based dipodal and tripodal alkoxide-based chelates as a route to structurally and magnetically interesting Mn clusters.

Introduction

There continues to be great interest in the study of polynuclear manganese complexes at intermediate oxidation states. The reasons for this continued interest include the architectural beauty such molecules often possess, their relevance to Mn biomolecules such as the photosynthetic oxygen-evolving center, and the intriguing property of Mn^{III}-containing clusters to often possess large, and sometimes abnormally large, ground-state spin (S) values. When the latter is combined with a significant and negative magnetoanisotropy (negative zero-field splitting parameter, D), single-molecule magnets (SMMs) result.[1] SMMs are molecular species that can function as nanoscale magnetic particles at sufficiently low temperatures because of a significant energy barrier to magnetization relaxation.[2] In addition, they display quantum effects such as quantum tunneling of the magnetization[3] and

*To whom correspondence should be addressed. E-mail: christou@chem.ufl.edu.

(1) For some representative references, see: (a) Christou, G.; Gatteschi, D.; Hendrickson, D. N.; Sessoli, R. *MRS Bull.* **2000**, *25*, 66. (b) Sessoli, R.; Tsai, H.-L.; Schake, A. R.; Wang, S.; Vincent, J. B.; Folting, K.; Gatteschi, D.; Christou, G.; Hendrickson, D. N. *J. Am. Chem. Soc.* **1993**, *115*, 1804.

(2) (a) Bircher, R.; Chaboussant, G.; Dobe, D.; Güdel, H. U.; Oshsenbein, S. T.; Sieber, A.; Waldmann, O. *Adv. Funct. Mater.* **2006**, *16*, 209. (b) Gatteschi, D.; Sessoli, R. *Angew. Chem., Int. Ed.* **2003**, *42*, 268. (c) Aubin, S. M. J.; Gilley, N. R.; Pardi, L.; Krzystek, J.; Wemple, M. W.; Brunel, L.-C.; Maple, M. B.; Christou, G.; Hendrickson, D. N. *J. Am. Chem. Soc.* **1998**, *120*, 4991. (d) Oshio, H.; Nakano, M. *Chem.—Eur. J.* **2005**, *11*, 5178.

(3) (a) Friedman, J. R.; Sarachik, M. P. *Phys. Rev. Lett.* **1996**, *76*, 3830. (b) Thomas, L.; Lionti, L.; Ballou, R.; Gatteschi, D.; Sessoli, R.; Barbara, B. *Nature* **1996**, *383*, 145.

Published on Web 09/18/2009

quantum phase interference.[4] As a result, SMMs represent potential molecular memory elements for specialized, molecule-based information storage devices and molecular spintronics,[5] as well as potential quantum bits for quantum information processing.[6]

The ability of clusters to possess large numbers of unpaired electrons is the primary focus of the present paper. Molecules with a large *S* are a fascinating area of importance to fields spanning chemistry, physics, materials science, and medicine. At one extreme is the fundamental desire to understand exactly how the sign and relative magnitudes of the constituent exchange interactions yield the high *S* value, whereas at the other are, for example, applications such as in MRI imaging and the SMM behavior mentioned above. For such reasons, we have a general interest in high-spin species and are seeking (i) new synthetic procedures to obtain such molecules using simple reagents;[7] (ii) to understand exactly how the large ground state *S* arises; and (iii) to attain some rudimentary level of control of *S* in such often high-nuclearity molecules.[8] If an obtained molecule also has a large *D* value, then its potential SMM properties are also of interest, but in fact complexes with the largest *S* values usually possess small *D* values,[9] as seen for $Mn_{28}Cu_{17}$, Mn_{25}, Mn_{19}, Mn_{17}, and Mn_{10} complexes with $S = 51/2$,[10] $51/2$[11] or $61/2$,[8a] $83/2$,[12] 37[13a] or 28 ± 1[13b] and 22[14] ground states, respectively.

Large *S* values can result from (a) ferro- or ferrimagnetic spin alignments and/or (b) competing interactions (spin frustration) in certain M_x topologies that prevent (frustrate) the preferred spin alignments.[15] In case (a), ferromagnetic interactions can result from ligands or structural characteristics known to give ferromagnetic coupling between metal centers. One of the best ferromagnetic couplers is the azide (N_3^-) group when it bridges metals in the 1,1-(end-on) fashion.[7,11−14,16] Others include pyridine-based alkoxide ligands,[8a,11,14a−14c,17] or diolate-[18] and triolate-based[10,12,14d,19] groups such as, *N*-methyldiethanolamine ($mdaH_2$) and triethanolamine ($teaH_3$), which are versatile chelating/bridging ligands whose bridging alkoxide arms often support ferromagnetic coupling. The rationalization of the observed ground state spins in purely ferromagnetic compounds is trivial, being the sum of the parallel-aligned individual spins. Similarly, purely ferrimagnetic complexes can be readily understood, being arrays of antiferromagnetically coupled metals with unequal single-ion spin values that lead to a significant net molecular spin *S*. In case (b), which includes the majority of polynuclear valence-trapped Mn clusters exhibiting a non-zero ground state, the molecular *S* value is a consequence of the many competing (predominantly) antiferromagnetic interactions that prevent (frustrate) perfectly antiparallel spin alignments. This is particularly true for antiferromagnetically coupled triangular M_3 subunits, since the spins cannot all be aligned antiparallel to both their neighbors. The ground state then becomes extremely difficult to predict from structural and simple spin-up/spin-down considerations. In fact, the net molecular *S* is dependent on the precise topology of the Mn_x framework and very sensitive to the relative strengths of the competing interactions. Crucial to the latter in mixed-valence Mn chemistry is the fact that $Mn^{II}-O-Mn^{III}$ and $Mn^{III}-O-Mn^{III}$ interactions are often of similar magnitude, either weakly antiferromagnetic or, occasionally, weakly ferromagnetic.[15] Thus, one of the major challenges in Mn

(4) (a) Wernsdorfer, W.; Sessoli, R. *Science* **2000**, 2417. (b) Wernsdorfer, W.; Soler, M.; Christou, G.; Hendrickson, D. N. *J. Appl. Phys.* **2002**, *91*, 7164. (c) Wernsdorfer, W.; Chakov, N. E.; Christou, G. *Phys. Rev. Lett.* **2005**, *95*, 037203 (1−4).

(5) Bogani, L.; Wernsdorfer, W. *Nature Mater.* **2008**, *7*, 179.

(6) Leuenberger, M. N.; Loss, D. *Nature* **2001**, *410*, 789.

(7) For a comprehensive review, see: Stamatatos, Th. C.; Christou, G. *Inorg. Chem.* **2009**, *48*, 3308, and references therein.

(8) (a) Stamatatos, Th. C.; Abboud, K. A.; Wernsdorfer, W.; Christou, G. *Angew. Chem., Int. Ed.* **2007**, *46*, 884. (b) Stamatatos, T. C.; Abboud, K. A.; Wernsdorfer, W.; Christou, G. *Polyhedron* **2007**, *26*, 2095. (c) Milios, C. J.; Inglis, R.; Vinslava, A.; Bagai, R.; Wernsdorfer, W.; Parsons, S.; Perlepes, S. P.; Christou, G.; Brechin, E. K. *J. Am. Chem. Soc.* **2007**, *129*, 12505. (d) For an excellent review, see: Milios, C. J.; Piligkos, S.; Brechin, E. K. *Dalton Trans.* **2008**, 1809.

(9) (a) Waldmann, O. *Inorg. Chem.* **2007**, *46*, 10035. (b) Ruiz, E.; Cirera, J.; Cano, J.; Alvarez, S.; Loose, C.; Kortus, J. *Chem. Commun.* **2008**, 52.

(10) Wang, W.- G.; Zhou, A.- J.; Zhang, W.- X.; Tong, M.- L.; Chen, X.- M; Nakano, M.; Beedle, C. C.; Hendrickson, D. N. *J. Am. Chem. Soc.* **2007**, *129*, 1014.

(11) (a) Murugesu, M.; Habrych, M.; Wernsdorfer, W.; Abboud, K. A.; Christou, G. *J. Am. Chem. Soc.* **2004**, *126*, 4766. (b) Murugesu, M.; Takahashi, S.; Wilson, A.; Abboud, K. A.; Wernsdorfer, W.; Hill, S.; Christou, G. *Inorg. Chem.* **2008**, *47*, 9459.

(12) (a) Ako, A. M.; Hewitt, I. J.; Mereacre, V.; Clérac, R.; Wernsdorfer, W.; Anson, C. E.; Powell, A. K. *Angew. Chem., Int. Ed.* **2006**, *45*, 4926. (b) Waldmann, O.; Ako, A. M.; Güdel, H. U.; Powell, A. K. *Inorg. Chem.* **2008**, *47*, 3486.

(13) (a) Moushi, E. E.; Stamatatos, Th. C.; Wernsdorfer, W.; Nastopoulos, V.; Christou, G.; Tasiopoulos, A. J. *Inorg. Chem.* **2009**, *48*, 5049. (b) Nayak, S.; Beltran, L. M. C.; Lan, Y.; Clérac, R.; Hearns, N. G. R.; Wernsdorfer, W.; Anson, C. E.; Powell, A. K. *Dalton Trans.* **2009**, 1901.

(14) (a) Stamatatos, Th. C.; Abboud, K. A.; Wernsdorfer, W.; Christou, G. *Angew. Chem., Int. Ed.* **2006**, *45*, 4134. (b) Stamatatos, Th. C.; Abboud, K. A.; Wernsdorfer, W.; Christou, G. *Polyhedron* **2007**, *26*, 2042. (c) Stamatatos, Th. C.; Poole, K. M.; Abboud, K. A.; Wernsdorfer, W.; O'Brien, T. A.; Christou, G. *Inorg. Chem.* **2008**, *47*, 5006. (d) Manoli, M.; Johnstone, R. D. L.; Parsons, S.; Murrie, M.; Affronte, M.; Evangelisti, M.; Brechin, E. K. *Angew. Chem., Int. Ed.* **2007**, *46*, 4456.

(15) (a) Kahn, O. *Molecular Magnetism*; VCH Publishers: New York, 1993. (b) Stamatatos, Th. C.; Christou, G. *Philos. Trans. R. Soc. A* **2008**, *366*, 113, and references cited therein.

(16) (a) Escuer, A.; Aromi, G. *Eur. J. Inorg. Chem.* **2006**, 4721, and references cited therein. (b) Ruiz, E.; Cano, J.; Alvarez, S.; Alemany, P. *J. Am. Chem. Soc.* **1998**, *120*, 11122.

(17) (a) Brechin, E. K.; Sanudo, E. C.; Wernsdorfer, W.; Boskovic, C.; Yoo, J.; Hendrickson, D. N.; Yamaguchi, A.; Ishimoto, H.; Concolino, T. E.; Rheingold, A. L.; Christou, G. *Inorg. Chem.* **2005**, *44*, 502. (b) Boudalis, A. K.; Donnadieu, B.; Nastopoulos, V.; Clemente-Juan, J. M.; Mari, A.; Sanakis, Y.; Tuchagues, J.- P.; Perlepes, S. P. *Angew. Chem., Int. Ed.* **2004**, *43*, 2266. (c) Papaefstathiou, G. S.; Perlepes, S. P.; Escuer, A.; Vicente, R.; Font-Bardia, M.; Solans, X. *Angew. Chem., Int. Ed.* **2001**, *40*, 884. (d) Papaefstathiou, G. S.; Escuer, A.; Vicente, R.; Font-Bardia, M.; Solans, X.; Perlepes, S. P. *Chem. Commun.* **2001**, 2414. (e) Stamatatos, Th. C.; Foguet-Albiol, D.; Stoumpos, C. C.; Raptopoulou, C. P.; Terzis, A.; Wernsdorfer, W.; Perlepes, S. P.; Christou, G. *J. Am. Chem. Soc.* **2005**, *127*, 15380. (f) Stamatatos, Th. C.; Foguet-Albiol, D.; Lee, S.- C.; Stoumpos, C. C.; Raptopoulou, C. P.; Terzis, A.; Wernsdorfer, W.; Hill, S.; Perlepes, S. P.; Christou, G. *J. Am. Chem. Soc.* **2007**, *129*, 9484. (g) Stamatatos, Th. C.; Abboud, K. A.; Wernsdorfer, W.; Christou, G. *Angew. Chem., Int. Ed.* **2008**, *47*, 6694. (h) Stamatatos, Th. C.; Efthymiou, C. G.; Stoumpos, C. C.; Perlepes, S. P. *Eur. J. Inorg. Chem.* **2009**, 3361.

(18) (a) Moushi, E. E.; Stamatatos, Th. C.; Wernsdorfer, W.; Nastopoulos, V.Christou, G.; Tasiopoulos, A. J. *Angew. Chem., Int. Ed.* **2006**, *45*, 7722. (b) Moushi, E. E.; Lampropoulos, C.; Wernsdorfer, W.; Nastopoulos, V.; Christou, G.; Tasiopoulos, A. J. *Inorg. Chem.* **2007**, *46*, 3795. (c) Foguet-Albiol, D.; O'Brien, T. A.; Wernsdorfer, W.; Moulton, B.; Zaworotko, M. J.; Abboud, K. A.; Christou, G. *Angew. Chem., Int. Ed.* **2005**, *44*, 897. (d) Shah, S. J.; Ramsey, C. M.; Heroux, K. J.; DiPasquale, A. G.; Dalal, N. S.; Rheingold, A. L.; del Barco, E.; Hendrickson, D. N. *Inorg. Chem.* **2008**, *47*, 9569. (e) Tasiopoulos, A. J.; Perlepes, S. P. *Dalton Trans.* **2008**, 5537, and references therein (Tutorial Review).

(19) (a) For a representative review, see: Brechin, E. K. *Chem. Commun.* **2005**, 5141, and references therein. (b) Scott, R. T. W.; Milios, C. J.; Vinslava, A.; Lifford, D.; Parsons, S.; Wernsdorfer, W.; Christou, G.; Brechin, E. K. *Dalton Trans.* **2006**, 3161. (c) Scott, R. T. W.; Parsons, S.; Murugesu, M.; Wernsdorfer, W.; Christou, G.; Brechin, E. K. *Angew. Chem., Int. Ed.* **2005**, *44*, 6540.

cluster chemistry is to rationalize exactly how the large ground state S of such often complicated complexes arises on the basis of the constituent spin frustration effects and the individual metal spin alignments that result. Here we report a study of some $Mn^{II}_4Mn^{III}_3$ complexes, and we shall show that we can rationalize both the origin of the $S = 11$ ground state normally observed, and the use of this knowledge to target and successfully attain an $S = 16$ variant with the maximum possible ground state spin. In addition, we also describe the fascinating supramolecular architectures that these clusters display. Portions of this work have been previously communicated.[20]

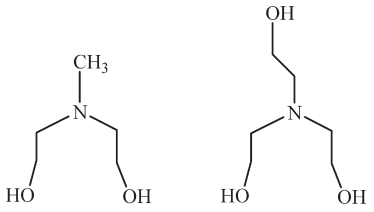

Experimental Section

Syntheses. All manipulations were performed under aerobic conditions using materials as received. ***Caution!*** *Although no such behavior was observed during the present work, perchlorate and azide salts are potentially explosive; such compounds should be synthesized and used in small quantities, and treated with utmost care at all times.*

$[Na(MeOH)_3][Mn_7(N_3)_6(mda)_6]$ (1). To a stirred solution of $mdaH_2$ (0.24 g, 2.0 mmol) and NEt_3 (0.28 mL, 2.0 mmol) in DMF/MeOH (25/5 mL) was added solid NaN_3 (0.07 g, 1.0 mmol). The mixture was stirred for a further 10 min and then solid $Mn(ClO_4)_2 \cdot 6H_2O$ (0.36 g, 1.0 mmol) was added, which caused a rapid color change from pale yellow to dark red. The solution was stirred for a further 1 h, filtered, and the filtrate layered with Et_2O (60 mL). After 4 days, X-ray quality dark-red crystals of **1**·MeOH were collected by filtration, washed with cold MeOH (2 × 3 mL) and Et_2O (2 × 5 mL), and dried in air; the yield was 55%. Anal. Calcd for **1** (solvent-free): C, 27.17; H, 5.39; N, 23.05%. Found: C, 27.12; H, 5.52; N, 23.14%. Selected IR data (cm^{-1}): 3431 (mb), 2956 (w), 2856 (m), 2056 (vs), 1594 (m), 1518 (m), 1456 (m), 1401 (m), 1336 (m), 1261 (m), 1202 (w), 1066 (m), 1032 (m), 999 (m), 912 (w), 888 (m), 760 (m), 735 (w), 670 (w), 644 (w), 580 (m), 442 (w).

$Na[Mn_7(N_3)_6(teaH)_6]$ (2). This complex was prepared in the same manner as complex **1** but using $teaH_3$ (0.30 g, 2.0 mmol) in place of $mdaH_2$. After 6 days, dark-red crystals of **2**·DMF·Et_2O were isolated, collected by filtration, washed with cold MeOH (2 × 3 mL) and Et_2O (2 × 5 mL), and dried under vacuum; the yield was 63%. Anal. Calcd for **2**·DMF: C, 28.99; H, 5.30; N, 21.67%. Found: C, 28.82; H, 5.19; N, 21.67%. Selected IR data (cm^{-1}): 3408 (mb), 2849 (m), 2071 (vs), 1672 (m), 1418 (w), 1383 (w), 1347 (w), 1268 (w), 1223 (w), 1063 (m), 1031 (m), 1000 (m), 892 (m), 777 (w), 588 (m), 525 (m).

$(NHEt_3)[Mn_7Cl_6(mda)_6]$ (3). To a stirred solution of $mdaH_2$ (0.06 g, 0.5 mmol) and NEt_3 (0.07 mL, 0.5 mmol) in MeCN (25 mL) was added solid $MnCl_2 \cdot 4H_2O$ (0.20 g, 1.0 mmol). The resulting brown slurry was stirred for 10 min and then refluxed for a further 2 h, during which time all solids dissolved. The dark brown solution was cooled down to room temperature, filtered, and the filtrate layered with Et_2O (50 mL). After 2 days, X-ray quality dark-red crystals of **3**·MeCN·Et_2O were collected by filtration, washed with cold MeCN (2 × 2 mL) and Et_2O (2 × 5 mL), and dried in air; the yield was 25%. Anal. Calcd for **3** (solvent-free): C, 30.83; H, 5.89; N, 6.99%. Found: C, 30.44; H, 6.10; N, 6.58%. Selected IR data (cm^{-1}): 3431 (mb), 2850 (m), 1652 (w), 1558 (w), 1456 (m), 1070 (s), 1039 (m), 1002 (w), 913 (w), 890 (m), 667 (w), 647 (w), 596 (w), 526 (w).

$(NHEt_3)[Mn_7(N_3)_6(mda)_6]$ (4). To a stirred solution of $mdaH_2$ (0.24 g, 2.0 mmol) and NEt_3 (0.28 mL, 2.0 mmol) in DMF/MeOH (25/5 mL) was added solid $NBu^n_4N_3$ (0.24 g, 1.0 mmol). The mixture was stirred for a further 20 min and then solid $Mn(ClO_4)_2 \cdot 6H_2O$ (0.36 g, 1.0 mmol) was added under vigorous stirring, which caused a rapid color change from pale yellow to dark red. The solution was stirred for a further 30 min, filtered, and the filtrate layered with Et_2O (60 mL). After 3 days, dark-red crystals were collected by filtration, washed with cold MeOH (2 × 3 mL) and Et_2O (2 × 5 mL), and dried under vacuum; the yield was 50%. Anal. Calcd for **4**: C, 29.99; H, 5.73; N, 24.29%. Found: C, 29.82; H, 5.59; N, 24.45%. Selected IR data (cm^{-1}): 3439 (mb), 2946 (m), 2876 (m), 2058 (vs), 1630 (m), 1616 (m), 1575 (m), 1540 (m), 1456 (m), 1419 (m), 1395 (m), 1296 (w), 1261 (w), 1205 (w), 1160 (w), 1066 (m), 1033 (m), 1002 (m), 890 (m), 802 (w), 746 (w), 667 (m), 647 (m), 596 (m), 526 (m), 442 (w).

$(NHEt_3)[Mn_7(N_3)_6(teaH)_6]$ (5). This complex was prepared in the same manner as complex **4** but using $teaH_3$ (0.30 g, 2.0 mmol) in place of $mdaH_2$. After 5 days, dark-red crystals were collected by filtration, washed with cold MeOH (2 × 3 mL) and Et_2O (2 × 5 mL), and dried under vacuum; the yield was 55%. Anal. Calcd for **5**: C, 31.10; H, 5.84; N, 21.59%. Found: C, 30.95; H, 5.67; N, 21.74%. Selected IR data (cm^{-1}): 3438 (mb), 2949 (m), 2866 (m), 2061 (vs), 1681 (m), 1423 (w), 1390 (w), 1356 (w), 1269 (w), 1227 (w), 1160 (w), 1061 (m), 1037 (m), 997 (m), 895 (m), 772 (w), 592 (m), 525 (m), 458 (w).

X-ray Crystallography. Data were collected on a Siemens SMART PLATFORM equipped with a CCD area detector and a graphite monochromator utilizing Mo Kα radiation (λ = 0.71073 Å). Suitable crystals of **1**·MeOH, **2**·DMF·Et_2O, and **3**·MeCN·Et_2O were attached to glass fibers using silicone grease and transferred to a goniostat where they were cooled to 173 K for data collection. An initial search for reciprocal space revealed a monoclinic cell for **1**·MeOH and **3**·MeCN·Et_2O, and a rhombohedral cell for **2**·DMF·Et_2O; space groups Cc (**1**·MeOH), $R3$ (**2**·DMF·Et_2O) and $P2_1/c$ (**3**·MeCN·Et_2O) were confirmed by the subsequent solution and refinement of the structures. Cell parameters were refined using up to 8192 reflections. A full sphere of data (1850 frames) was collected using the ω-scan method (0.3° frame width). The first 50 frames were remeasured at the end of data collection to monitor instrument and crystal stability (maximum correction on I was $< 1\%$). Absorption corrections by integration were applied based on measured indexed crystal faces. The structures were solved by direct methods in SHELXTL6,[21] and refined on F^2 using full-matrix least-squares. The non-H atoms were treated anisotropically, whereas the H atoms were placed in calculated, ideal positions and refined as riding on their respective C atoms.

For **1**·MeOH, the asymmetric unit consists of the complete Mn_7 cluster, a sodium cation, and four MeOH molecules. All four MeOH hydroxyl protons were located in a difference Fourier map and refined freely. One of the azide ligands has its two terminal N atoms disordered and was refined in two parts. A total of 758 parameters were included in the structure refinement using 7270 reflections with $I > 2\sigma(I)$ to yield R1 and wR2 of 4.29 and 9.90%, respectively.

(20) Stamatatos, Th. C.; Poole, K. M.; Foguet-Albiol, D.; Abboud, K. A.; O'Brien, T. A.; Christou, G. *Inorg. Chem.* **2008**, *47*, 6593.

(21) *SHELXTL6*; Bruker-AXS: Madison, WI, 2000.

Table 1. Crystallographic Data for **1**·MeOH, **2**·DMF·Et_2O, and **3**·MeCN·Et_2O

parameter	**1**	**2**	**3**
formula[a]	$C_{34}H_{82}N_{24}O_{16}Mn_7Na$	$C_{41}H_{95}N_{25}O_{20}Mn_7Na$	$C_{42}H_{95}N_8O_{13}Cl_6Mn_7$
fw, g mol^{-1}[a]	1490.81	1665.99	1517.54
crystal system	monoclinic	rhombohedral	monoclinic
space group	*Cc*	*R*3	$P2_1/c$
a, Å	17.2034(8)	15.8536(6)	11.1009(7)
b, Å	15.4286(7)	15.8536(6)	19.0949(12)
c, Å	22.9340(11)	22.7938(12)	29.2126(19)
β, deg	98.398(1)	90	97.502(2)
V, $Å^3$	6022.0(5)	4961.4(4)	6139.2(7)
Z	4	3	4
T, K	173(2)	173(2)	173(2)
radiation, Å[b]	0.71073	0.71073	0.71073
ρ_{calc}, g cm^{-3}	1.644	1.673	1.642
μ, mm^{-1}	1.507	1.386	1.716
R1[c,d]	0.0429	0.0348	0.0655
*w*R2[e]	0.0990	0.0906	0.1678

[a] Including solvate molecules. [b] Graphite monochromator. [c] $I > 2\sigma(I)$. [d] $R1 = \sum||F_o| - |F_c||/\sum|F_o||$. [e] $wR2 = [\sum w(F_o^2 - F_c^2)^2/\sum w(F_o^2)^2]^{1/2}$, $w = 1/[\sigma^2(F_o^2) + [(ap)^2 + bp]$, where $p = [\max(F_o^2, 0) + 2F_c^2]/3$.

For **2**·DMF·Et_2O, the asymmetric unit consists of a 1/3 Mn_7 cluster, a sodium cation, and 1/3 DMF and 1/3 Et_2O molecules of crystallization, all lying on 3-fold rotation axes. The two solvent molecules are disordered and could not be modeled properly; thus, program SQUEEZE,[22] a part of the PLATON package of crystallographic software, was used to calculate the solvent disorder area and remove its contribution to the overall intensity data. The protons on O5 and O6 were located in a difference Fourier map and refined riding on their parent O atoms. A total of 259 parameters were included in the structure refinement on F^2 using 4422 reflections with $I > 2\sigma(I)$ to yield R1 and wR2 of 3.48 and 9.06%, respectively.

For **3**·MeCN·Et_2O, the asymmetric unit consists of the complete Mn_7 cluster, a triethylammonium cation, and MeCN and Et_2O molecules of crystallization. The latter two could not be modeled properly, thus the program SQUEEZE was again used to calculate the solvent disorder area and remove its contribution to the overall intensity data. A total of 627 parameters were included in the final cycle of refinement on F^2 using 39381 reflections with $I > 2\sigma(I)$ to yield R1 and wR2 of 6.55 and 16.78%, respectively.

Unit cell data and details of the structure refinements for the three complexes are collected in Table 1.

Physical Measurements. Infrared spectra were recorded in the solid state (KBr pellets) on a Nicolet Nexus 670 FTIR spectrometer in the 4000−450 cm^{-1} range. Elemental analyses (C, H, and N) were performed on a Perkin-Elmer 2400 Series II Analyzer. Variable-temperature direct current (dc) and alternating current (ac) magnetic susceptibility data were collected at the University of Florida using a Quantum Design MPMS-XL SQUID susceptometer equipped with a 7 T magnet and operating in the 1.8−300 K range. Samples were embedded in solid eicosane to prevent torquing. The ac magnetic susceptibility measurements were performed in an oscillating ac field of 3.5 Oe and a zero dc field. The oscillation frequencies were in the 5−1488 Hz range. Magnetization versus field and temperature data were fit using the program MAGNET.[23] Pascal's constants were used to estimate the diamagnetic corrections, which were subtracted from the experimental susceptibilities to give the molar paramagnetic susceptibilities (χ_M). Low-temperature (< 1.8 K) hysteresis studies and dc relaxation measurements were performed at Grenoble using an array of micro-SQUIDS.[24] The high sensitivity of this magnetometer allows the study of single crystals of SMMs of the order of 10−500 μm. The field can be applied in any direction by separately driving three orthogonal coils. Crystals were maintained in mother liquor to avoid degradation and were covered in grease for protection during the transfer to the micro-SQUID and subsequent cooling.

Theoretical Calculations. The exchange constants in complexes **1** and **2** were estimated with the ZILSH method[25] and density functional theory (DFT) calculations. For the ZILSH calculations, unrestricted Hartree−Fock molecular orbital wave functions were obtained with the INDO/S method of Zerner[26] for various spin components of the complex in which the spins of certain metals are reversed relative to the others. These wave functions were assumed to follow an effective Heisenberg spin Hamiltonian given by eq 1, where A and B label metal centers and

$$\check{H}_{\text{eff}} = \check{H}_0 - 2\sum_{A<B} J_{AB}\hat{S}_A\cdot\hat{S}_B \quad (1)$$

$\check{H}_0$ contains all spin-independent terms in the electronic Hamiltonian. The expectation value of $\check{H}_{\text{eff}}$ for a spin component wave function ψ_i is given by eq 2, where E_0 contains all spin-

$$E^{\text{UHF},i} = E_0 - 2\sum_{A<B} J_{AB}\langle\hat{S}_A\cdot\hat{S}_B\rangle^{\text{UHF},i} \quad (2)$$

independent contributions to the energy. Spin couplings $\langle\hat{S}_A\cdot\hat{S}_B\rangle^{\text{UHF}}$ were calculated with the semiempirical local spin operator of Davidson and O'Brien.[27] Given energies and spin couplings for the appropriate number of spin components, eqs 2 were solved simultaneously for the parameters E_0 and J_{AB} for all unique combinations of A and B. The spin components used were the ones with all unpaired spins aligned parallel, and all the other components with unpaired spins on all unique combinations of two metal ions reversed.

(22) Van der Sluis, P.; Spek, A. L. *Acta Crystallogr., Sect. A: Found. Crystallogr.* **1990**, *A46*, 194.
(23) Davidson, E. R. *MAGNET*; Indiana University: Bloomington, IN, 1999.
(24) Wernsdorfer, W. *Adv. Chem. Phys.* **2001**, *118*, 99.
(25) O'Brien, T. A.; Davidson, E. R. *Int. J. Quantum Chem.* **2003**, *92*, 294.
(26) (a) Zerner, M. C.; Loew, G. H.; Kirchner, R. F.; Muellerwesterhoff, U. T. *J. Am. Chem. Soc.* **1980**, *102*, 589. (b) Ridley, J. E.; Zerner, M. C. *Theor. Chim. Acta* **1973**, *32*, 111. (c) Kotzian, M.; Rosch, N.; Zerner, M. C. *Theor. Chim. Acta* **1992**, *81*, 201. (d) Culberson, J. C.; Knappe, P.; Rosch, N.; Zerner, M. C. *Theor. Chim. Acta* **1987**, *71*, 21. (e) Cory, M. G.; Kostlmeier, S.; Kotzian, M.; Rosch, N.; Zerner, M. C. *J. Chem. Phys.* **1994**, *100*, 1353. (f) Bacon, A. D.; Zerner, M. C. *Theor. Chim. Acta* **1979**, *53*, 21. (g) Anderson, W. P.; Cundari, T. R.; Zerner, M. C. *Int. J. Quantum Chem.* **1991**, *39*, 31. (h) Anderson, W. P.; Cundari, T. R.; Drago, R. S.; Zerner, M. C. *Inorg. Chem.* **1990**, *29*, 1.
(27) (a) Davidson, E. R.; Clark, A. E. *Mol. Phys.* **2002**, *100*, 373. (b) Clark, A. E.; Davidson, E. R. *J. Chem. Phys.* **2001**, *115*, 7382.

A similar strategy was used in the DFT calculations by assuming that energies of unrestricted Kohn−Sham determinants representing the spin components also follow eqs 2. Following our standard procedure, ZILSH spin couplings were used with DFT energies to obtain estimates of the exchange constants. Spin couplings computed with the ZILSH method are generally similar to those obtained from DFT densities.[28] The B3LYP functional[29] was used for all DFT calculations, which were performed with the Gaussian03 program.[30] Two basis sets were employed, either the triple-ζ TZVP basis set of Alrichs[31] for Mn atoms and the double-ζ DZVP basis set of Alrichs[32] for lighter atoms (basis set I), or the triple-ζ TZVP basis set of Alrichs[31] on all atoms (basis set II). An important quantity obtained from both ZILSH and DFT calculations was the local spin density for each metal atom, equal to the number of unpaired electrons (N_i) on metal atom "i".[25] The signs of the N_i indicate the spin alignments within the complex for a particular spin component. The local spin densities were used to check that the correct spin component densities were obtained from the calculations.

Once the exchange constants (J_{AB}) were obtained, wave functions and energies of the spin eigenstates described by the Heisenberg spin model could be obtained by substituting the J_{AB} into the Heisenberg spin Hamiltonian (eq 1 with $\hat{H}_0 = 0$) and diagonalizing the operator in the basis of spin components $\phi_i = |M_1M_2 \cdots M_N\rangle_i$, where M_A is the formal local z component of spin of metal "A" (i.e., $M_A = {}^5/_2$ for high spin d^5 Mn^{II} ions, $M_A = 2$ for high spin d^4 Mn^{III} ions). The wave functions of the spin eigenstates are then linear combinations of the basis functions ϕ_i,

$$|\Psi_s\rangle = \sum_i C_i\phi_i = \sum_i C_i|M_1M_2\cdots M_N\rangle_i \qquad (3)$$

as given by eq 3. In the case of a ground state with non-zero spin, the component making the leading contribution to the wave function (i.e., that with the largest weighting coefficient C_i) indicates the spin alignments in the ground state. Complexes **1** and **2** are too large to be treated with full matrix diagonalization, so the more efficient Davidson algorithm[33] was used to extract the energy for the lowest energy state of each spin. The spin components employed, their calculated energies, and the spin densities at each Mn atom are listed in Supporting Information, Tables S2 and S3 for **1** and **2**, respectively.

Results and Discussion

Syntheses. Synthetic procedures to Mn clusters are available involving the reaction of an alcohol-containing chelate with a simple Mn^{II} salt or a higher oxidation state source. With carboxylates, pyridyl alcohols such as 2-(hydroxymethyl)pyridine (hmpH), 2-(hydroxyethyl)-pyridine (hepH), and 2,6-pyridinedimethanol ($pdmH_2$) have given products such as $[Mn_{10}O_4(OH)_2(O_2CMe)_8(hmp)_8]^{4+}$,[34] $[Mn_{18}O_{14}(O_2CMe)_{18}(hep)_4(hepH)_2(H_2O)_2]^{2+}$,[17a] and $[Mn_4(O_2CMe)_2(pdmH)_6]^{2+}$,[35] respectively, whereas ligands such as 1,1,1-tris(hydroxymethyl)ethane ($thmeH_3$), $teaH_3$, propane-1,3-diol, and $mdaH_2$ have led to various rod-like[36] and loop-shaped[18] manganese carboxylate clusters. In contrast, the present study has avoided the presence of carboxylate ligands and has instead focused on the combination of a chelate and Cl^- or N_3^- ions.

A variety of reactions differing in the Cl^- or N_3^- amount, the other inorganic ions present, the Mn/$mdaH_2$(or $teaH_3$)/NEt_3 ratio, and/or the solvent were explored in identifying the following successful systems. Reaction of $Mn(ClO_4)_2$, $mdaH_2$, NEt_3 and NaN_3 (1:2:2:1) in DMF/MeOH gave the one-dimensional (1-D) polymer $[Na(MeOH)_3][Mn_7(N_3)_6(mda)_6]$ (**1**), as summarized in eq 4.

$$7Mn^{2+} + 6mdaH_2 + 9NEt_3 + Na^+ + 6N_3^- + 3/4O_2 + 3MeOH \rightarrow [Na(MeOH)_3][Mn_7(N_3)_6(mda)_6] + 9NHEt_3^+ + 3/2H_2O \qquad (4)$$

The same procedure used with $teaH_3$ instead of $mdaH_2$ gave instead a three-dimensional (3-D) coordination polymer $Na[Mn_7(N_3)_6(teaH)_6]$ (**2**), as in eq 5.

$$7Mn^{2+} + 6teaH_3 + 9NEt_3 + Na^+ + 6N_3^- + 3/4O_2 \rightarrow Na[Mn_7(N_3)_6(teaH)_6] + 9NHEt_3^+ + 3/2H_2O \qquad (5)$$

Both reactions involve Mn oxidation, undoubtedly by O_2 under the prevailing basic conditions, and have been balanced accordingly. The NEt_3 both ensures basic conditions and acts as a proton acceptor; in its absence, longer reaction times (> 24 h) are required to get a significant dark red coloration, and the yields of isolated **1** and **2** are much lower (< 10%). On the other hand, > 2 equiv of NEt_3 gave oily products suggestive of mixtures that we have not been able to characterize, or insoluble amorphous precipitates that were probably Mn oxides or oxo/hydroxides. Increase in the amount of the $mdaH_2$ or $teaH_3$ to 3 equiv (or more) also led to isolation of **1** or **2** but in low yields of 5−12%.

Reaction products can often be solvent-dependent in 3d cluster chemistry,[19a,14c,37] we therefore explored the reactions in neat DMF but found little difference: the products were $[Na(H_2O)_3][Mn_7(N_3)_6(mda)_6]$, containing

(28) Davidson, E. R.; Clark, A. E. *J. Phys. Chem. A* **2002**, *106*, 7456.
(29) (a) Lee, C.; Yang, W.; Parr, R. G. *Phys. Rev. B* **1988**, *37*, 785. (b) Becke, A. D. *J. Chem. Phys.* **1993**, *98*, 5648.
(30) Frisch, M. J.; Trucks, G. W.; Schlegel, H. B.; Scuseria, G. E.; Robb, M. A.; Cheeseman, J. R.; Montgomery, J. A., Jr.; Vreven, T.; Kudin, K. N.; Burant, J. C.; Millam, J. M.; Iyengar, S. S.; Tomasi, J.; Barone, V.; Mennucci, B.; Cossi, M.; Scalmani, G.; Rega, N.; Petersson, G. A.; Nakatsuji, H.; Hada, M.; Ehara, M.; Toyota, K.; Fukuda, R.; Hasegawa, J.; Ishida, M.; Nakajima, T.; Honda, Y.; Kitao, O.; Nakai, H.; Klene, M.; Li, X.; Knox, J. E.; Hratchian, H. P.; Cross, J. B.; Adamo, C.; Jaramillo, J.; Gomperts, R.; Stratman, R. E.; Yazyev, O.; Austin, A. J.; Cammi, R.; Pomell, C.; Ochterski, J. W.; Ayala, P. Y.; Morokuma, K.; Voth, G. A.; Salvador, P.; Dannenberg, J. J.; Zakrzewski, V. G.; Dapprich, S.; Daniels, A. D.; Strain, M. C.; Farkas, O.; Malick, D. K.; Rabuck, A. D.; Raghavachari, K.; Foresman, J. B.; Ortiz, J. V.; Cui, Q.; Baboul, A. G.; Clifford, S.; Cioslowski, J.; Stefanov, B. B.; Liu, G.; Liashenko, A.; Piskorz, P.; Komaromi, I.; Martin, R. L.; Fox, D. J.; Keith, T.; Al-Laham, M. A.; Peng, C. Y.; Nanayakkara, A.; Challacombe, M.; Gill, P. M. W.; Johnson, B.; Chen, W.; Wong, M. W.; Gonzalez, C.; Pople, J. A. *Gaussian03*, Revision B.05; Gaussian, Inc.: Pittsburgh, PA, 2003.
(31) Schaefer, A.; Horn, H.; Ahlrichs, R. *J. Chem. Phys.* **1994**, *100*, 5829.
(32) Schaefer, A.; Horn, H.; Ahlrichs, R. *J. Chem. Phys.* **1992**, *97*, 2571.
(33) Davidson, E. R. *J. Comput. Phys.* **1975**, *17*, 87.
(34) Harden, N. C.; Bolcar, M. A.; Wernsdorfer, W.; Abboud, K. A.; Streib, W. E.; Christou, G. *Inorg. Chem.* **2003**, *42*, 7067.
(35) Yoo, J.; Brechin, E. K.; Yamaguchi, A.; Nakano, M.; Huffman, J. C.; Maniero, A. L.; Brunel, L.-C.; Awaga, K.; Ishimoto, H.; Christou, G.; Hendrickson, D. N. *Inorg. Chem.* **2000**, *39*, 3615.
(36) Rajaraman, G.; Murugesu, M.; Sanudo, E. C.; Soler, M.; Wernsdorfer, W.; Helliwell, M.; Muryn, C.; Raftery, J.; Teat, S. J.; Christou, G.; Brechin, E. K. *J. Am .Chem. Soc.* **2004**, *126*, 15445.
(37) Brockman, J. T.; Stamatatos, Th. C.; Wernsdorfer, W.; Abboud, K. A.; Christou, G. *Inorg. Chem.* **2007**, *46*, 9160.

H_2O at the MeOH positions of **1**, and complex **2**, in the same or slightly higher yields (~65−70%). Similarly, MeCN/MeOH also gave **1** and **2** but in lower yields and purity. In contrast, the use of neat MeOH as solvent did not give **1** and **2** but $[Mn^{II}_2Mn^{III}_2(N_3)_4(mda)_2(mdaH)_2]$,[38] with the common diamond-shaped Mn_4 core, and a mixture of **2** and another product currently under characterization. Non-polar solvents such as CH_2Cl_2 and $CHCl_3$ required much longer reaction times and gave **1** and **2** in very low yields (< 5%) as the only isolable products.

Since the Na^+ ions in **1** and **2** lead to polymeric products, we also sought the corresponding products with organic cations. The same reactions employing $NBu^n_4N_3$ instead of NaN_3 successfully led to isolation of $(NHEt_3)[Mn_7(N_3)_6(mda)_6]$ (**4**) and $(NHEt_3)[Mn_7(N_3)_6(teaH)_6]$ (**5**). We did not obtain good enough crystals for X-ray crystallography, but their identity was deduced by elemental analyses and the similarity of their IR spectra and magnetic properties to those of **1**−**3** (vide infra).

When NaN_3 was omitted from the reactions that give **1** and **2**, we were unable to isolate any pure material for characterization. However, when we explored the use of $MnCl_2 \cdot 4H_2O$ in place of both $Mn(ClO_4)_2 \cdot 6H_2O$ and NaN_3 (and thus in the absence of Na^+) in a reaction with $mdaH_2$ and NEt_3 in various ratios, we found that the 2:1:1 reaction led to isolation of pure dark-red crystals of $(NHEt_3)[Mn_7Cl_6(mda)_6]$ (**3**), as summarized in eq 6.

$$7Mn^{2+} + 6mdaH_2 + 9NEt_3 + 6Cl^- + 3/4O_2 \rightarrow [Mn_7Cl_6(mda)_6]^- + 9NHEt_3^+ + 3/2H_2O \quad (6)$$

The corresponding $teaH^{2-}$ complex, $(NHEt_3)[Mn_7Cl_6(teaH)_6]$, was obtained from the analogous reaction with $teaH_3$ in place of $mdaH_2$.

Description of Structures. The structures of the anions of **1**−**3** are shown in Figure 1, and selected interatomic distances and angles are listed in Table 2. The three anions all contain a near-planar hexagon of alternating Mn^{II} and Mn^{III} atoms surrounding a central, seventh Mn^{II} atom. This Mn_7 unit is held together by 12 O atoms of six η^2:η^1:η^3:μ_4 bridging mda^{2-} ligands (for **1** and **3**) or six η^2:η^1:η^3:μ_4 bridging $teaH^{2-}$ ligands (for **2**). There are six μ_3-O atoms bridging the Mn_6 hexagon with the central Mn atom, and six μ-O atoms bridging Mn_2 pairs of the hexagon. Peripheral ligation is completed by six terminal N_3^- (in **1** and **2**) or Cl^- (in **3**) ions and six N atoms from the corresponding mda^{2-} (in **1** and **3**) or $teaH^{2-}$ (in **2**) groups. The $[Mn_7(\mu_3\text{-}OR)_6(\mu\text{-}OR)_6]^{5+}$ core of **1**−**3** contains an exactly or near-planar Mn_7 unit (Figure 2), with the displacement of the central Mn atom from the Mn_6 least-squares plane being 0.075 Å in **1** and 0.098 Å in **2**, but zero in **3** since the central Mn lies in the Mn_6 plane; this small difference probably reflects the structural difference between **1**/**2** and **3** in that the anions of the former are linked via Na^+ cations, which likely imposes small distortions on the repeating units. The core can alternatively be described as consisting of six $\{Mn_3O_4\}$ partial-cubane units, each doubly face-sharing, and all six vertex-sharing at the central Mn^{II} atom. Figure 2 also emphasizes that **1**−**3** have a layered structure, with layers of O atoms above and below the Mn_7 plane, reminiscent of the hexagonal close-packed two-dimensional (2-D) structure in CdI_2, for example.[39]

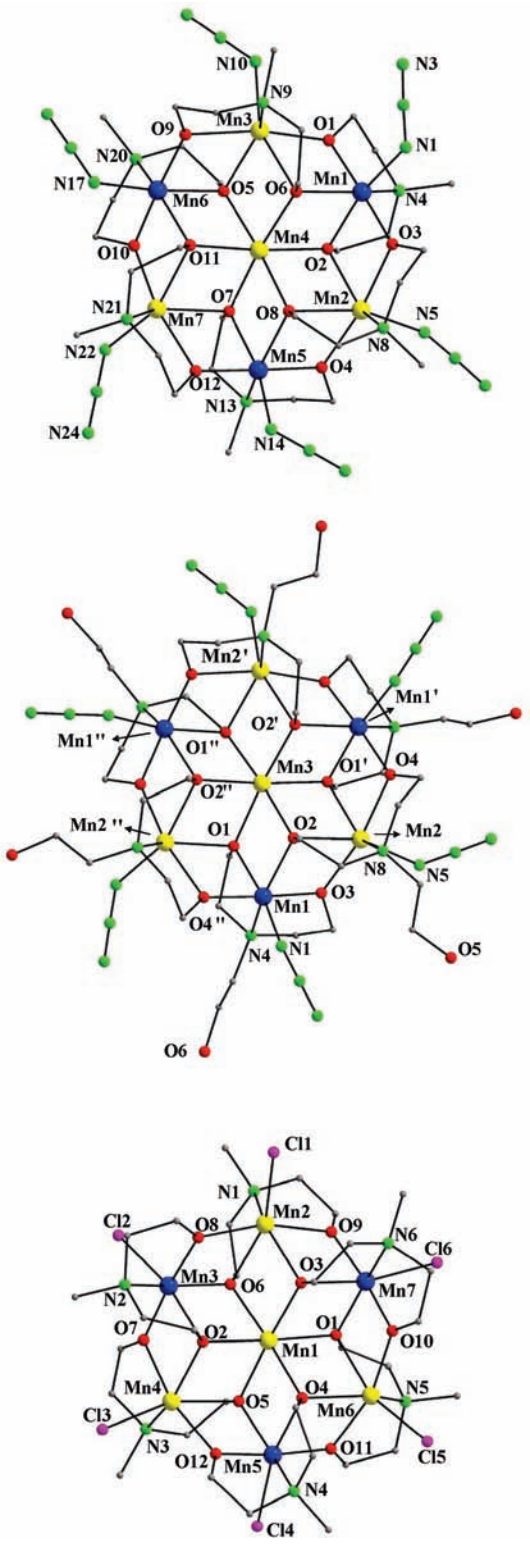

Figure 1. Labeled PovRay representations of the anions of complexes **1** (top), **2** (middle), and **3** (bottom), with H atoms omitted for clarity. Color scheme: Mn^{II} yellow; Mn^{III} blue; Cl purple; O red; N green; C gray.

(38) Taguchi, T.; Abboud, K. A.; Christou, G., to be submitted.

(39) *Inorganic Structural Chemistry*; Muller, U., Ed.; Wiley: New York, 1993.

Table 2. Selected Interatomic Distances (Å) and Angles (deg) for **1**·MeOH, **2**·DMF·Et_2O, and **3**·MeCN·Et_2O

1·MeOH

Mn(1)···Mn(2)	3.302(1)	Mn(3)···Mn(6)	3.305(2)
Mn(1)···Mn(3)	3.313(2)	Mn(4)···Mn(5)	3.338(1)
Mn(1)···Mn(4)	3.297(2)	Mn(4)···Mn(6)	3.300(2)
Mn(2)···Mn(4)	3.299(2)	Mn(4)···Mn(7)	3.291(2)
Mn(2)···Mn(5)	3.315(2)	Mn(5)···Mn(7)	3.305(2)
Mn(3)···Mn(4)	3.324(1)	Mn(6)···Mn(7)	3.310(1)
Mn(1)−O(1)	1.896(4)	Mn(4)−O(7)	2.196(4)
Mn(1)−O(2)	2.103(4)	Mn(4)−O(8)	2.188(4)
Mn(1)−O(3)	1.875(4)	Mn(4)−O(11)	2.188(4)
Mn(1)−O(6)	2.156(4)	Mn(5)−O(4)	1.908(4)
Mn(1)−N(1)	2.025(5)	Mn(5)−O(7)	2.088(4)
Mn(1)−N(4)	2.279(6)	Mn(5)−O(8)	2.187(4)
Mn(2)−O(2)	2.248(4)	Mn(5)−O(12)	1.886(4)
Mn(2)−O(3)	2.142(4)	Mn(5)−N(13)	2.321(6)
Mn(2)−O(4)	2.116(4)	Mn(5)−N(14)	1.985(6)
Mn(2)−O(8)	2.271(4)	Mn(6)−O(5)	2.068(4)
Mn(2)−N(5)	2.133(6)	Mn(6)−O(9)	1.891(4)
Mn(2)−N(8)	2.297(6)	Mn(6)−O(10)	1.894(4)
Mn(3)−O(1)	2.135(4)	Mn(6)−O(11)	2.152(4)
Mn(3)−O(5)	2.238(4)	Mn(6)−N(17)	2.024(6)
Mn(3)−O(6)	2.243(4)	Mn(6)−N(20)	2.293(6)
Mn(3)−O(9)	2.176(4)	Mn(7)−O(7)	2.250(4)
Mn(3)−N(9)	2.309(5)	Mn(7)−O(10)	2.112(4)
Mn(3)−N(10)	2.169(5)	Mn(7)−O(11)	2.278(4)
Mn(4)−O(2)	2.195(4)	Mn(7)−O(12)	2.155(4)
Mn(4)−O(5)	2.240(4)	Mn(7)−N(21)	2.286(6)
Mn(4)−O(6)	2.197(4)	Mn(7)−N(22)	2.146(6)
Mn(1)−O(1)−Mn(3)	110.4(2)	Mn(3)−O(6)−Mn(4)	96.9(2)
Mn(1)−O(2)−Mn(2)	98.7(2)	Mn(3)−O(9)−Mn(6)	108.5(2)
Mn(1)−O(2)−Mn(4)	100.2(2)	Mn(5)−O(7)−Mn(4)	102.4(2)
Mn(1)−O(3)−Mn(2)	110.4(2)	Mn(5)−O(7)−Mn(7)	99.2(2)
Mn(1)−O(6)−Mn(3)	97.7(2)	Mn(5)−O(8)−Mn(4)	99.5(2)
Mn(1)−O(6)−Mn(4)	98.5(2)	Mn(5)−O(12)−Mn(7)	109.5(2)
Mn(2)−O(2)−Mn(4)	95.9(2)	Mn(6)−O(5)−Mn(4)	99.9(2)
Mn(2)−O(4)−Mn(5)	110.8(2)	Mn(6)−O(10)−Mn(7)	111.3(2)
Mn(2)−O(8)−Mn(4)	95.4(2)	Mn(6)−O(11)−Mn(4)	99.0(2)
Mn(2)−O(8)−Mn(5)	96.1(2)	Mn(6)−O(11)−Mn(7)	96.7(2)
Mn(3)−O(5)−Mn(4)	95.8(2)	Mn(7)−O(7)−Mn(4)	95.5(2)
Mn(3)−O(5)−Mn(6)	100.2(2)	Mn(7)−O(11)−Mn(4)	94.9(2)

2·DMF·Et_2O[a]

Mn(1)···Mn(2)	3.324(1)	Mn(1)···Mn(3)	3.302(1)
Mn(1′)···Mn(2)	3.300(1)	Mn(2)···Mn(3)	3.324(1)
Mn(1)−O(1)	2.050(2)	Mn(2)−O(2)	2.250(2)
Mn(1)−O(2)	2.192(2)	Mn(2)−O(3)	2.106(2)
Mn(1)−O(3)	1.905(2)	Mn(2)−O(4)	2.124(2)
Mn(1)-O(4″)	1.889(2)	Mn(2)−N(5)	2.161(3)
Mn(1)−N(1)	1.990(3)	Mn(2)−N(8)	2.322(3)
Mn(1)−N(4)	2.349(2)	Mn(3)−O(1)	2.223(2)
Mn(2)-O(1′)	2.274(2)	Mn(3)−O(2)	2.177(2)
Mn(1)−O(1)−Mn(2″)	99.4(1)	Mn(1)−O(3)−Mn(2)	111.9(1)
Mn(1)−O(1)−Mn(3)	101.1(1)	Mn(1′)-O(4)−Mn(2)	110.5(1)
Mn(1)−O(2)−Mn(2)	96.9(9)	Mn(2″)-O(1)−Mn(3)	95.3(9)
Mn(1)−O(2)−Mn(3)	98.2(9)	Mn(2)−O(2)−Mn(3)	97.3(9)

3·MeCN·Et_2O

Mn(1)···Mn(2)	3.331(1)	Mn(2)···Mn(3)	3.301(1)
Mn(1)···Mn(3)	3.276(1)	Mn(2)···Mn(7)	3.337(1)
Mn(1)···Mn(4)	3.305(1)	Mn(3)···Mn(4)	3.324(1)
Mn(1)···Mn(5)	3.291(1)	Mn(4)···Mn(5)	3.303(1)
Mn(1)···Mn(6)	3.359(1)	Mn(5)···Mn(6)	3.310(1)
Mn(1)···Mn(7)	3.277(1)	Mn(6)···Mn(7)	3.287(1)
Mn(1)−O(1)	2.258(5)	Mn(4)−O(12)	2.112(5)
Mn(1)−O(2)	2.196(5)	Mn(4)−N(3)	2.290(7)
Mn(1)−O(3)	2.172(6)	Mn(4)−Cl(3)	2.499(2)
Mn(1)−O(4)	2.177(5)	Mn(5)−O(4)	2.146(6)
Mn(1)−O(5)	2.238(6)	Mn(5)−O(5)	2.085(5)
Mn(1)−O(6)	2.224(5)	Mn(5)−O(11)	1.876(6)
Mn(2)−O(3)	2.192(5)	Mn(5)−O(12)	1.899(5)
Mn(2)−O(6)	2.306(6)	Mn(5)−N(4)	2.233(7)
Mn(2)−O(8)	2.128(6)	Mn(5)−Cl(4)	2.412(3)
Mn(2)−O(9)	2.162(6)	Mn(6)−O(1)	2.340(6)
Mn(2)−N(1)	2.291(7)	Mn(6)−O(4)	2.203(5)
Mn(2)−Cl(1)	2.437(3)	Mn(6)−O(10)	2.099(6)
Mn(3)−O(2)	2.223(5)	Mn(6)−O(11)	2.150(6)
Mn(3)−O(6)	2.037(5)	Mn(6)−N(5)	2.292(7)
Mn(3)−O(7)	1.879(6)	Mn(6)−Cl(5)	2.424(3)
Mn(3)−O(8)	1.905(6)	Mn(7)−O(1)	2.039(6)
Mn(3)−N(2)	2.171(7)	Mn(7)−O(3)	2.200(5)
Mn(3)−Cl(2)	2.423(2)	Mn(7)−O(9)	1.901(6)
Mn(4)−O(2)	2.184(6)	Mn(7)−O(10)	1.886(5)
Mn(4)−O(5)	2.280(5)	Mn(7)−N(6)	2.187(8)
Mn(4)−O(7)	2.154(5)	Mn(7)−Cl(6)	2.462(3)
Mn(1)−O(1)−Mn(6)	93.8(2)	Mn(2)−O(3)−Mn(7)	98.9(2)
Mn(1)−O(1)−Mn(7)	99.2(2)	Mn(2)−O(9)−Mn(7)	110.3(3)
Mn(1)−O(2)−Mn(3)	95.7(2)	Mn(2)−O(6)−Mn(3)	98.8(2)
Mn(1)−O(2)−Mn(4)	98.0(2)	Mn(2)−O(8)−Mn(3)	109.7(3)
Mn(1)−O(3)−Mn(2)	99.5(2)	Mn(3)−O(2)−Mn(4)	97.9(2)
Mn(1)−O(3)−Mn(7)	97.1(2)	Mn(3)−O(7)−Mn(4)	110.8(3)
Mn(1)−O(4)−Mn(5)	99.1(2)	Mn(4)−O(5)−Mn(5)	98.2(2)
Mn(1)−O(4)−Mn(6)	100.1(2)	Mn(4)−O(12)−Mn(5)	110.7(2)
Mn(1)−O(5)−Mn(4)	94.0(2)	Mn(5)−O(4)−Mn(6)	99.1(2)
Mn(1)−O(5)−Mn(5)	99.1(2)	Mn(5)−O(11)−Mn(6)	110.4(3)
Mn(1)−O(6)−Mn(2)	94.6(2)	Mn(6)−O(1)−Mn(7)	97.0(2)
Mn(1)−O(6)−Mn(3)	100.4(2)	Mn(6)−O(10)−Mn(7)	111.0(3)

[a] Unprimed, primed, and double-primed atoms are related by the 3-fold symmetry.

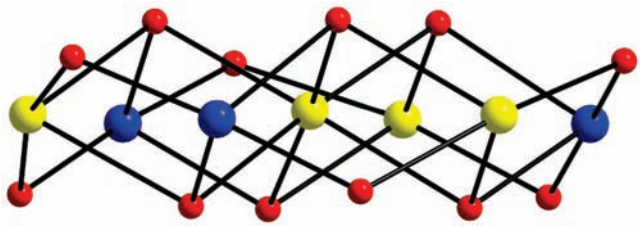

Figure 2. PovRay representation of the $[Mn_7(\mu_3\text{-}OR)_6(\mu\text{-}OR)_6]^{5+}$ core. The view is from the side to emphasize the alternating O/Mn/O layered structure. Color scheme: Mn^{II} yellow; Mn^{III} blue; O red.

The Mn atoms are all six-coordinate with near-octahedral geometry. The oxidation state assignments mentioned above were determined from charge considerations, the metric parameters, bond valence sum (BVS)[40] calculations (Supporting Information, Table S1), and the identification of Jahn−Teller (JT) distortions expected for Mn^{III} ions; the Mn_7 anions of **1**−**3** are thus mixed-valent $4Mn^{II}$, $3Mn^{III}$ and they are color-coded accordingly in Figure 1. The protonation levels of the bound O atoms were confirmed by O BVS calculations (Supporting Information, Table S1) to be deprotonated. The Mn^{III} JT elongation axes are O(2)−Mn(1)−N(1), O(8)−Mn(5)−N(13), and O(11)−Mn(6)−N(20) for **1**, O(2)−Mn(1)−N(4) for **2**, and O(2)−Mn(3)−Cl(2), O(4)−Mn(5)−Cl(4), and O(3)−Mn(7)−Cl(6) for **3**, each involving one of the μ_3-O atoms of the mda^{2-} or $teaH^{2-}$ ligands. The Mn_7 anions have virtual or imposed C_3 symmetry.

In **1** and **2**, the Mn_7 anions are connected by the Na^+ cations into 1-D and 3-D supramolecular assemblies, respectively. In **1**, the $[Na(MeOH)_3]^+$ becomes five-coordinate with distorted trigonal bipyramidal geometry (τ = 0.74, where τ is 0 and 1 for ideal square pyramidal

(40) (a) Brown, I. D.; Altermatt, D. *Acta Crystallogr.* **1985**, *B41*, 244. (b) Liu, W.; Thorp, H. H. *Inorg. Chem.* **1993**, *32*, 4102.

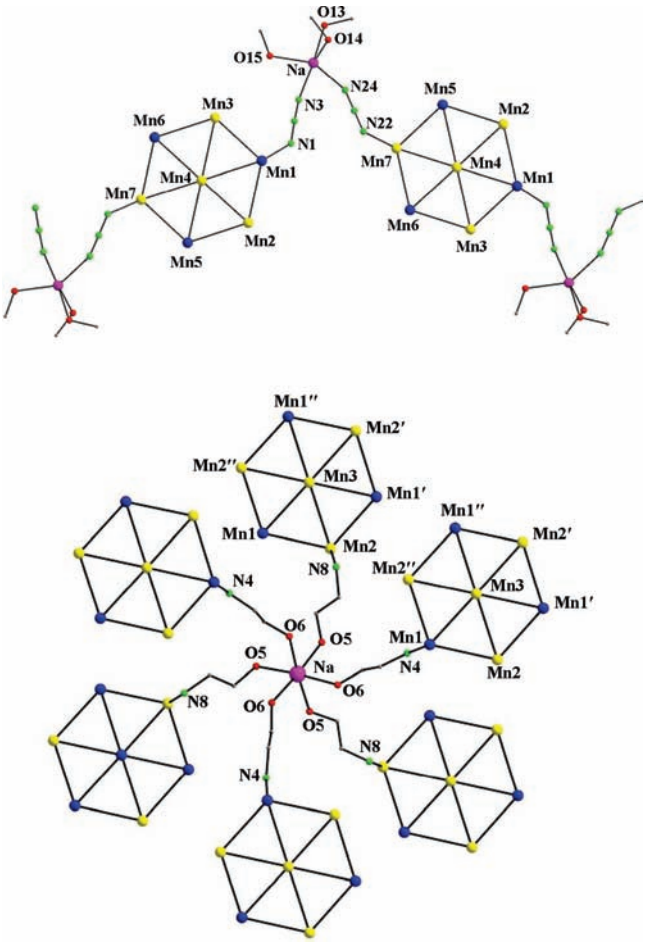

Figure 3. Supramolecular assembly of the Mn_7 anions of **1** (top) and **2** (bottom) through Na^+ linkages. Black lines between Mn atoms indicate the $Mn^{2+}\cdots Mn^{3+}$ and $Mn^{2+}\cdots Mn^{2+}$ vectors. Color scheme: Mn^{II} yellow; Mn^{III} blue; Na^I purple; O red; N green; C gray.

and trigonal bipyramidal geometries)[41] by bonding to two azide N atoms (N3, N24) of two adjacent Mn_7 anions, giving a zig-zagging chain (Figure 3, top). Each chain is then hydrogen-bonded to adjacent chains on each side, via $MeOH\cdots N_3^-$ and $MeOH\cdots MeOH\cdots N_3^-$ hydrogen-bonds, the latter including the lattice MeOH molecule. This gives a 2-D sheet structure possessing a herringbone pattern (Supporting Information, Figure S1), with only weak interactions between neighboring sheets. In **2**, the Na^+ ion forms six symmetry-equivalent bonds to the unbound, protonated alcohol arms of $teaH^{2-}$ groups from six neighboring Mn_7 anions (Figure 3, bottom), three above and three below the octahedral Na^+ ion. In addition, the three $teaH^{2-}$ groups of each Mn_7 anion bind to a different Na^+ ion, giving a 3-D network consisting of planes of Mn7 anions sandwiching the Na^+ ions (Supporting Information, Figure S2). In contrast, complex **3** consists of discrete ion-pairs of Mn_7 anions each hydrogen-bonded to a $NHEt_3^+$ cation through a terminal Cl^- ligand (N7$\cdots$Cl3 = 3.140(9) Å). Note that the nature of the linkage of **1** into a chain provides a reasonable superexchange ($Mn-N_3-Na-N_3-Mn$) pathway for inter-Mn_7 interactions, which are likely to be weak, since they are through a diamagnetic Na^+ cation, but perhaps still significant. This is, in fact, what is observed (vide infra). In contrast, the nature of the inter-Mn_7 linkage in **2** via the $teaH^{2-}$ alcohol arms suggests only very weak superexchange interactions, and again this is consistent with the experimental results below.

Complexes **1**−**3** join a family of known Mn_7 clusters that span only a few structural types, and these are collected in Table 3 for convenient comparison of structural and magnetic data (vide infra). Although there are a number of disk-like Mn_7 complexes now known, complexes **1** and **2** are nevertheless the first to crystallize as interesting supramolecular assemblies as a result of the Na^+ cations, and in fact they are very rare examples of high-nuclearity Mn clusters covalently linked through diamagnetic Na^+ ions.[18a,b,42]

Magnetochemistry

dc Magnetic Susceptibility Studies of 1, 3, and 4. Variable-temperature, solid-state magnetic susceptibility measurements were performed on powdered microcrystals, restrained in eicosane to prevent torquing, in a 1 kOe (0.1 T) field and in the 5.0−300 K range. The obtained data are shown as $\chi_M T$ versus T plots in Figure 4. $\chi_M T$ for **1** steadily increases from 26.15 cm^3 K mol^{-1} at 300 K to a maximum of 65.81 cm^3 K mol^{-1} at 6.5 K and then decreases very slightly to 65.78 cm^3 K mol^{-1} at 5.0 K; the latter is likely due to a combination of Zeeman effects, zero-field splitting (ZFS), and weak intermolecular interactions mediated by the Na^+ ions. The $\chi_M T$ plot for **3** is almost superimposable with that of **1**, increasing from 23.66 cm^3 K mol^{-1} at 300 K to a maximum of 64.54 cm^3 K mol^{-1} at 6.5 K and then decreasing very slightly to 64.49 cm^3 K mol^{-1} at 5.0 K. The 300 K values are essentially equal to the spin-only ($g = 2$) value of 26.5 cm^3 K mol^{-1} for four Mn^{II} and three Mn^{III} non-interacting ions, and the steady increase with decreasing temperature is consistent with dominant ferromagnetic exchange interactions within the Mn_7 anions and a resulting large ground state spin S value. The $\chi_M T$ versus T plot for **4** (Supporting Information, Figure S3) is very similar to those for **1** and **3**, steadily increasing from 24.60 cm^3 K mol^{-1} at 300 K to a maximum of 67.12 cm^3 K mol^{-1} at 8.0 K and then decreasing to 67.06 cm^3 K mol^{-1} at 5.0 K. The ~5.0 K values for **1**, **3**, and **4** are suggestive of an $S = 11$ ground state with g slightly less than 2.0, as expected for Mn^{III}-containing systems.

To confirm the suggested $S = 11$ ground state of **1** and **3** and to determine the magnitude of D, magnetization (M) versus dc field measurements were made for restrained samples at applied magnetic fields (H) and temperatures of 1−50 kOe and 1.8−10.0 K, respectively. The resulting data are shown in Figure 5 as reduced magnetization ($M/N\,\mu_B$) versus H/T plots, where N is Avogadro's number and μ_B is the Bohr magneton. The experimental isofield data for **1** and **3** in Figure 5 clearly do not superimpose, indicating significant magnetic anisotropy (ZFS) in the ground state. The data were fit by matrix diagonalization, using the program MAGNET,[23]

(41) Addison, A. W.; Rao, T. N.; Reedijk, J.; Rijn, J.; Verschoor, G. C. *J. Chem. Soc., Dalton Trans.* **1984**, 1349.

(42) Murugesu, M.; Wernsdorfer, W.; Abboud, K. A.; Brechin, E. K.; Christou, G. *Dalton Trans.* **2006**, 2285.

Table 3. Structural Types and Ground State S Values for Mn_7 Clusters

complex [a,b]	core	type	S	U_{eff} [c]	ref
$[Mn^{II}_7(OH)_2(O_2CMe)_4(trz)_8]_n$	$[Mn_7(\mu_3{-}OH)_2(\mu\text{-}NN)_8]^{4+}$	d	nr		43
$[Mn^{II}_7(L)_6(H_2O)_{2.25}(MeOH)_{0.75}]^{2+}$	$[Mn_7(\mu\text{-}OR)_6]^{2+}$	e	nr		44
$[Mn^{II}Mn^{III}_6O_2(O_2CMe)_6(Et\text{-}sao)_6]^{2-}$	$[Mn_7(\mu_3\text{-}O)_2(\mu_3\text{-}ON)_6]^{10+}$	f	$^{13}/_2$	nr	45
$[Mn^{II}Mn^{III}_6O_2(O_2CMe)_5(Et\text{-}sao)_6(solv)_2]^{-}$	$[Mn_7(\mu_3\text{-}O)_2(\mu_3\text{-}ON)_6]^{10+}$	f	$^{11}/_2$	32	45
$[Mn^{II}Mn^{III}_6O_4(O_2CMe)_8(trien)_2(dien)_2]^{4+}$	$[Mn_7(\mu_3\text{-}O)_4]^{12+}$	g	nr		46
$[Mn^{II}_2Mn^{III}_5O_2(O_2CPh)_9(thme)_2(py)_3]$	$[Mn_7(\mu_3\text{-}O)_2(\mu_3\text{-}OR)_3(\mu\text{-}OR)_3]^{9+}$	h	7		36
$[Mn^{II}_2Mn^{III}_4Mn^{IV}O_3(O_3PPh)_3(O_2CBu^t)_8(py)_3]$	$[Mn_7(\mu_3\text{-}O)_3]^{14+}$	i	$^{13}/_2$		47
$[Mn^{II}_3Mn^{III}_4(5\text{-}NO_2\text{-}hbide)_6]$	$[Mn_7(\mu_3\text{-}OR)_6(\mu\text{-}OR)_6]^{6+}$	j	$^{19}/_2$	18.1	48
$[Mn^{II}_3Mn^{III}_4(OMe)_{12}(dbm)_6]$	$[Mn_7(\mu_3\text{-}OMe)_6(\mu\text{-}OMe)_6]^{6+}$	j	$^{17}/_2$	nr	49
$[Mn^{II}_4Mn^{III}_3Cl_6(L')_6]^{-}$	$[Mn_7(\mu_3\text{-}OR)_6(\mu\text{-}OR)_6]^{5+}$	j	nr	nr	50
$[Mn^{II}_4Mn^{III}_3(tea)_3(teaH)_3]^{2+}$	$[Mn_7(\mu_3\text{-}OR)_6(\mu\text{-}OR)_6]^{5+}$	j	11	19.5	51
$[Mn^{II}_4Mn^{III}_3(OH)_3Cl_3(hmp)_9]^{2+}$	$[Mn_7(\mu_3{-}OH)_3(\mu_3\text{-}OR)_3(\mu\text{-}OR)_6]^{5+}$	j	11		34
$[Mn^{II}_4Mn^{III}_3(N_3)_6(mda)_6]^{-}$ (**1** and **4**)	$[Mn_7(\mu_3\text{-}OR)_6(\mu\text{-}OR)_6]^{5+}$	j	11		tw
$[Mn^{II}_4Mn^{III}_3(N_3)_6(teaH)_6]^{-}$ (**2** and **5**)	$[Mn_7(\mu_3\text{-}OR)_6(\mu\text{-}OR)_6]^{5+}$	j	16		tw
$[Mn^{II}_4Mn^{III}_3Cl_6(mda)_6]^{-}$ (**3**)	$[Mn_7(\mu_3\text{-}OR)_6(\mu\text{-}OR)_6]^{5+}$	j	11		tw
$[Mn^{III}_3Mn^{IV}_4O_8(O_2SePh)_8(O_2CMe)(H_2O)]$	$[Mn_7(\mu_3\text{-}O)_5(\mu\text{-}O)_3]^{9+}$	k	2	14.2	52
$[Mn^{III}_3Mn^{IV}_4O_8(O_2SePh)_9(H_2O)]$	$[Mn_7(\mu_3\text{-}O)_5(\mu\text{-}O)_3]^{9+}$	k	2	nr	52

[a] Counterions and solvate molecules are omitted. [b] Abbreviations: nr = not reported; tw = this work; trzH = 1,2,4-triazole; LH_2 = tetradentate imino-carboxylate ligand; Et-saoH_2 = 2-hydroxypropiophenone oxime; trien = triethylenetetramine; dien = diethylenetriamine; py = pyridine; 5-NO_2-hbideH_3 = N-(2-hydroxy-5-nitrobenzyl)iminodiethanol; dbmH = dibenzoylmethane; L′H_2 = N-substituted diethanolamines. [c] For SMMs (in Kelvin units); a blank entry denotes non-SMM behavior. [d] Two linked triads. [e] A twisted Mn_6 trigonal-prismatic cage around a central capped Mn atom. [f] Distorted bitetrahedron. [g] Two linked $[Mn_4(\mu_3\text{-}O)_2]^{7+}$ butterflies. [h] Five edge-sharing triangles. [i] A linked $[Mn_3(\mu_3\text{-}O)]^{7+}$ triangle with a $[Mn_4(\mu_3\text{-}O)_2]^{7+}$ butterfly. [j] Disk-like. [k] Two Mn^{IV}_2 dimers attached to a central $[Mn_3(\mu_3\text{-}O)_4]^{+}$ unit.

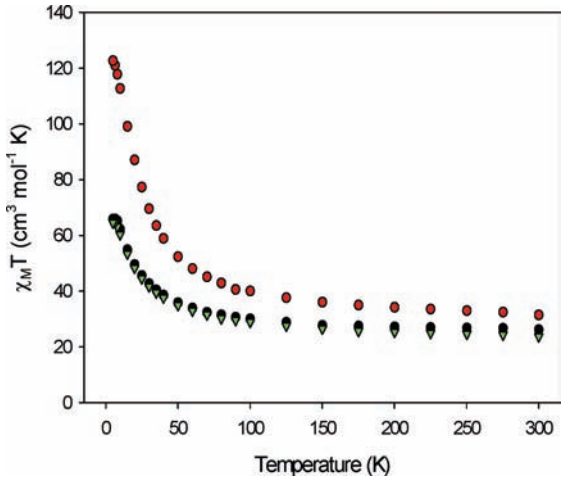

Figure 4. $\chi_M T$ vs T plots for complexes **1** (black circles), **2**·DMF (red circles), and **3** (green triangles) in a 1 kG dc field.

to a model that assumes only the ground state is populated, includes isotropic Zeeman interactions and axial ZFS ($D\hat{S}_z^2$), and incorporates a full powder average. The corresponding spin Hamiltonian is given by eq 7, where $\hat{S}_z$ is the easy-axis spin operator, and μ_0 is the vacuum

$$\mathscr{H} = D\hat{S}_Z^2 + g\mu_B\mu_0\hat{S}\cdot H \qquad (7)$$

permeability. The last term is the Zeeman energy associated with an applied magnetic field. We could not obtain good fits using data collected in the full field range up to 70 kOe (7 T). The observation that the plots would not saturate but instead were continuing to increase with increasing fields was suggestive of low-lying excited states being the cause of the bad fits. This is consistent with the high content of Mn^{II} in these complexes, which give weak exchange coupling and thus low-lying excited states. This is a common problem and can often be circumvented by using only data collected at lower fields. Indeed, when data for **1** and **3** only up to 2 T were employed, satisfactory fits were now obtained. These are shown as solid lines in Figure 5, and the fit parameters were $S = 11$, $g = 1.95$, $D = -0.15$ cm^{-1} for **1**, and $S = 11$, $g = 1.92$, $D = -0.13$ cm^{-1} for **3**. The fit for **1** is still not good, and as we shall show below, this is because it also undergoes significant intermolecular interactions through the linking Na^+ cation. Alternative fits with $S = 10$ or 12 were rejected because they gave unreasonably large and small values of g, respectively.

The small D values obtained for **1** and **3** are consistent with the structures of the Mn_7 anions. The main source of molecular anisotropy is the three JT distorted Mn^{III} ions, and the projections of these single-ion anisotropies onto the molecular anisotropy axis will be the main contributors to the molecular D value. As described above, the three Mn^{III} JT elongation axes are O(2)−Mn(1)−N(1), O(8)−Mn(5)−N(13), and O(11)−Mn(6)−N(20) for **1**, and O(2)−Mn(3)−Cl(2), O(4)−Mn(5)−Cl(4), and O(3)−Mn(7)−Cl(6) for **3**, which are disposed in a propeller-like fashion and lie almost in the Mn_7 planes. Thus, the projections of these onto the molecular z (virtual C_3) axis will give a small net molecular axial anisotropy (D).[10,14,53] Electron paramagnetic resonance (EPR) spectroscopic studies on the related $[Mn^{II}_4Mn^{III}_3(tea)_3(teaH)_3]^{2+}$ complex have given a similarly small $D = -0.08$ cm^{-1}.[51]

ac Magnetic Susceptibility Studies. As an independent probe of the ground state S, and as a means of investigating the magnetization relaxation dynamics, we investigated complexes **1**−**5** by ac magnetic susceptibility studies. The large $S = 11$ ground state of **1** and **3** together with their small but negative D suggested they might possess a big enough barrier (U) to magnetization relaxation to be SMMs. As mentioned, the upper limit to U for an integer spin is given by $U = S^2|D| = 121|D|$ for **1** and **3**, giving $U \sim 16{-}18$ cm^{-1}, but the actual or effective barrier (U_{eff}) will be less because of Quantum Tunnelling of Magnetization (QTM) through the barrier.

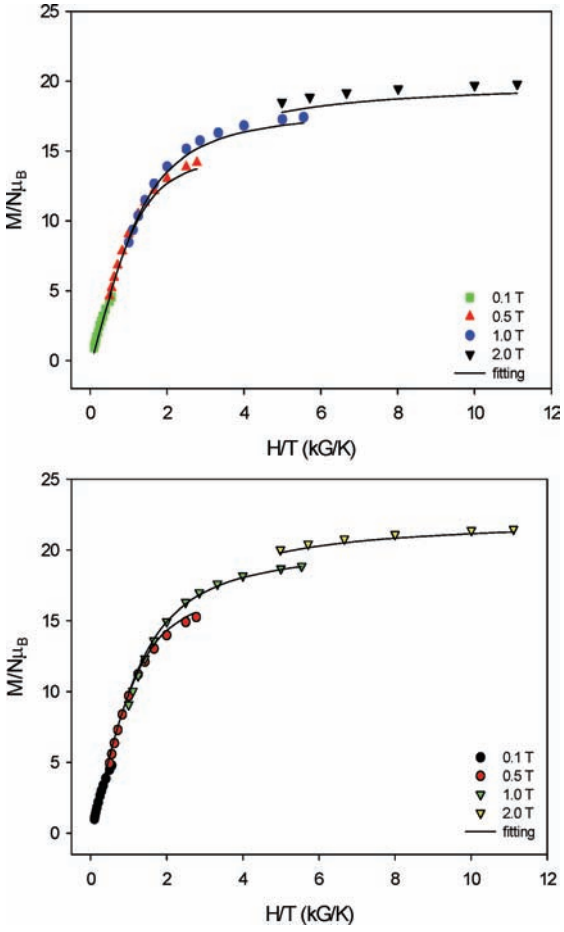

Figure 5. Plot of reduced magnetization ($M/N\mu_B$) vs H/T for complex **1** (top) and complex **3** (bottom) at applied fields of 0.1−2.0 T and in the 1.8−10 K temperature range. The solid lines are the fit of the data; see the text for the fit parameters.

The ac studies were performed in the 1.8−15 K range using a 3.5 Oe field oscillating at frequencies in the 5−1500 Hz range. If the magnetization vector can stay in phase with the oscillating field, then there is no imaginary (out-of-phase) susceptibility signal (χ''_M), and the real (in-phase) susceptibility (χ'_M) is equal to the dc susceptibility.[54] However, if the barrier to magnetization relaxation is significant compared to thermal energy (kT), then there is a non-zero χ''_M signal and the in-phase signal decreases, suggesting an SMM.[18a,52,55] For complex **1**, the in-phase $\chi'_M T$ signal above ~5 K slowly increases with decreasing temperature (Figure 6, top), before reaching a plateau and then decreasing at the lowest temperatures, primarily because of intermolecular interactions, both dipolar and superexchange. Extrapolating the plot from above 5 to 0 K gives ~55 cm^3 K mol^{-1}, consistent with an $S = 11$ ground state but only if g is ~1.83. This is in contrast to the dc plot of Figure 4, which shows a low temperature maximum of ~66 cm^3 K mol^{-1}, and we believe this is due to intermolecular antiferromagnetic interactions in **1** via the Na^+ linkage; their effect is overcome by the applied dc field in the dc studies, but in the ac studies they serve to decrease the observed $\chi'_M T$ signal slightly. It thus became important to obtain the $\chi'_M T$ versus T plot for $(NHEt_3)[Mn_7(N_3)_6(mda)_6]$ (**4**), effectively complex **1** without the Na^+ linkages and thus with only the weaker intermolecular interactions typical of large S molecules in the solid state, and this is shown in Figure 6, bottom; the $\chi'_M T$ values are now much higher than for **1**, and extrapolation of the data from above 5 to 0 K gives $\chi'_M T \sim 65$ cm^3 K mol^{-1}, as expected for $S = 11$ and $g \sim 2$. Similar behavior was observed for $(NHEt_3)[Mn_7Cl_6(mda)_6]$ (**3**) in Figure 6, middle, whose slightly increasing $\chi'_M T$ with decreasing temperature above 5 K extrapolates to ~65 cm^3 K mol^{-1} at 0 K, again indicating an $S = 11$ ground state. Thus, although the stronger-than-normal intermolecular interactions in **1** complicate matters a little, the combined dc and ac data nevertheless indicate that complexes **1**, **3**, and **4** all possess $S = 11$ ground states.

None of the decreases in $\chi'_M T$ in Figure 6 below ~5 K display the frequency-dependence of a SMM, and that is why they are assigned to anisotropy and weak intermolecular interactions. In accord with this, complexes **1** and **3** display essentially no out-of-phase χ''_M signals down to 1.8 K, only the merest hint of frequency-dependent tails of peaks that clearly lie at much lower temperatures (Supporting Information, Figure S4). Complex **4** showed no χ''_M signal down to 1.8 K.

Theoretical Studies: Rationalization of the $S = 11$ Ground States of 1, 3, and 4. An $S = 11$ ground state has now been identified for five Mn_7 complexes at the $Mn^{II}_4Mn^{III}_3$ oxidation level: **1**, **3**, **4**, and the two previously published examples $[Mn^{II}_4Mn^{III}_3(tea)_3(teaH)_3]^{2+}$ and $[Mn^{II}_4Mn^{III}_3(OH)_3Cl_3(hmp)_9]^{2+}$ in Table 3. We found this repeated occurrence of $S = 11$ surprising. In complexes containing only $Mn^{II}Mn^{II}$ and $Mn^{II}Mn^{III}$ interactions, all the interactions would be expected to be weak and of comparable magnitude.[15,56] Therefore, since the Mn_7 topology consists of fused Mn_3 triangles, common examples of units susceptible to spin frustration

(43) Quellette, W.; Prosvirin, A. V.; Valeich, J.; Dunbar, K. M.; Zubieta, J. *Inorg. Chem.* **2007**, *46*, 9067.
(44) Doble, D. M. J.; Benison, C. H.; Blake, A. J.; Fenske, D.; Jackson, M. S.; Kay, R. D.; Li, W.- S.; Schröder, M. *Angew. Chem., Int. Ed.* **1999**, *38*, 1915.
(45) Milios, C. J.; Gass, I. A.; Vinslava, A.; Budd, L.; Parsons, S.; Wernsdorfer, W.; Perlepes, S. P.; Christou, G.; Brechin, E. K. *Inorg. Chem.* **2007**, *46*, 6215.
(46) Bhula, R.; Weatherburn, D. C. *Angew. Chem., Int. Ed.* **1991**, *30*, 688.
(47) Shanmugam, M.; Chastanet, G.; Mallah, T.; Sessoli, R.; Teat, S. J.; Timco, G. A.; Winpenny, R. E. P. *Chem.—Eur. J.* **2006**, *12*, 8777.
(48) Koizumi, S.; Nihei, M.; Shiga, T.; Nakano, M.; Nojiri, H.; Bircher, R.; Waldmann, O.; Ochsenbein, S. T.; Güdel, H. U.; Fernandez-Alonso, F.; Oshio, H. *Chem.—Eur. J.* **2007**, *13*, 8445.
(49) Abbati, G. L.; Cornia, A.; Fabretti, A.; Caneschi, A.; Gatteschi, D. *Inorg. Chem.* **1998**, *37*, 3759.
(50) Saalfrank, R. W.; Nakajima, T.; Mooren, N.; Scheurer, A.; Maid, H.; Hampel, F.; Trienflinger, C.; Daub, J. *Eur. J. Inorg. Chem.* **2005**, 1149.
(51) Pilawa, B.; Kelemen, M. T.; Wanka, S.; Geisselmann, A.; Barra, A. L. *Europhys. Lett.* **1998**, *43*, 7.
(52) Chakov, N. E.; Wernsdorfer, W.; Abboud, K. A.; Christou, G. *Inorg. Chem.* **2004**, *43*, 5919.
(53) (a) Tsai, H.- L.; Wang, S.; Folting, K.; Streib, W. E.; Hendrickson, D. N.; Christou, G. *J. Am. Chem. Soc.* **1995**, *117*, 301. (b) King, P.; Wernsdorfer, W.; Abboud, K. A.; Christou, G. *Inorg. Chem.* **2005**, *44*, 8659. (c) Aromi, G.; Knapp, M. J.; Claude, J.- P.; Huffman, J. C.; Hendrickson, D. N.; Christou, G. *J. Am. Chem. Soc.* **1999**, *121*, 5489.
(54) Novak, M. A.; Sessoli, R. In *Quantum Tunnelling of Magnetization*, QTM'94; Gunther, L., Barbar, B., Eds.; Kluwer: Dordrecht, The Netherlands, 1995; pp 171−188.
(55) Mishra, A.; Tasiopoulos, A. J.; Wernsdorfer, W.; Abboud, K. A.; Christou, G. *Inorg. Chem.* **2007**, *46*, 3105.
(56) Que, L., Jr.; True, A. E. *Prog. Inorg. Chem.* **1990**, *38*, 97.

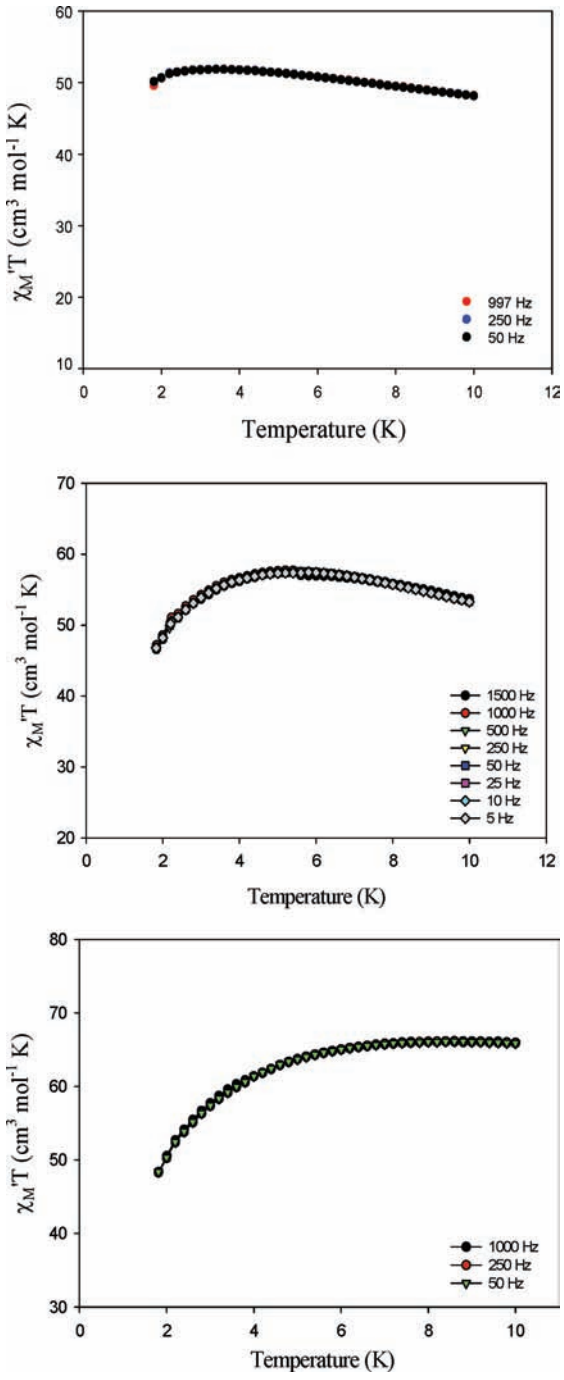

Figure 6. Plots of the ac in-phase $\chi'_M T$ vs T for complexes **1** (top), **3** (middle), and **4** (bottom) at the indicated frequencies.

effects, it would be reasonable to conclude that the ground state would be very sensitive to the relative magnitudes of the competing interactions; an Mn^{II}_4-Mn^{III}_3 species could have a ground state spin in the $S = 0-16$ range, so an intermediate $S = 11$ value could be rationalized as due to spin frustration.[15] Thus, a family of several Mn_7 complexes might be expected to display a variety of spin ground states resulting from small differences in their exchange parameters due to small differences in their structural parameters, from differing ligation, crystal packing, solvation, and so forth. However, the above five Mn_7 complexes instead all possess the same $S = 11$ ground states even though they span a range of ligand sets. It thus seemed of importance to understand the origin of the $S = 11$ ground state, and whether, for example, there really are spin frustration effects operating. To do this, we required access to the constituent exchange parameters. Unfortunately, the Mn_7 complexes are not amenable to the Kambe method[57] and neither is it easy to obtain them reliably by fitting of the VT magnetization data for such a complicated high nuclearity Mn system. Therefore, we obtained them from theoretical calculations using ZILSH and DFT methods.

Calculations were carried out by DFT on the complete anion of the representative $S = 11$ complex **1** using the crystallographic coordinates and spin couplings obtained with the semiempirical ZILSH method.[25] ZILSH calculations were performed on 22 spin components so that estimates of all parameters in eq 2 could be obtained (E_0 and 21 pairwise exchange constants). The components used included the one with all unpaired spins aligned parallel ("high spin", HS), and all components with the spin on two metal ions flipped and thus antiparallel to the others (e.g., Mn1 and Mn2 flipped, Mn1 and Mn3 flipped, etc.). The calculated energies and local Mn spin densities for each component are presented in Supporting Information, Table S2. The spin densities are close to the formal values of five and four expected for high-spin Mn^{2+} (d^5) and Mn^{3+} (d^4), respectively, but are reduced below these numbers by spin delocalization, as found with ZILSH for other complexes.[14c,25,58] The signs of the local spin densities indicate the relative directions of the spin moments of the Mn ions, and show that correct spin distributions were obtained for all spin components considered.

The exchange constants J_{AB} were obtained for **1** from the data of Supporting Information, Table S2 by simultaneous solution of eqs 2. The obtained values are listed in Table 4, together with the calculated spin couplings $\langle \hat{S}_A \cdot \hat{S}_B \rangle$, and together they explain the experimentally observed $S = 11$ ground state of **1** on the basis of spin frustration, as shown in Figure 7, top. The outer Mn^{2+}/Mn^{3+} interactions ($J_{23(o)}$) are all ferromagnetic and significantly stronger than the inner Mn^{2+}/Mn^{2+} ($J_{22(i)}$) and Mn^{2+}/Mn^{3+} ($J_{23(i)}$) interactions, and these fix all the outer spins in a parallel alignment. The alignment of the central Mn^{2+} spin is thus determined solely by the different sign and relative magnitude of $J_{22(i)}$ and $J_{23(i)}$; for **1**, the antiferromagnetic $J_{22(i)}$ is the stronger, frustrating the ferromagnetic $J_{23(i)}$ and aligning the central spin antiparallel to the outer hexagon, giving an $S = {}^{27}/_2 - {}^{5}/_2 = 11$ ground state (Figure 7, top).

The spin alignments in the ground state of **1** are confirmed by the calculated spin couplings $\langle \hat{S}_A \cdot \hat{S}_B \rangle$ (Table 4). These can be compared with those predicted by eq 8 for two spins S_A and S_B coupled together to give a total spin S_T. For a Mn^{2+}/Mn^{2+} or Mn^{2+}/Mn^{3+} pair aligned perfectly

$$\langle \hat{S}_A \cdot \hat{S}_B \rangle = \frac{1}{2}[S_T(S_T+1) - S_A(S_A+1) - S_B(S_B+1)] \quad (8)$$

(57) Kambe, K. *J. Phys. Soc. Jpn.* **1950**, *5*, 48.
(58) (a) Stamatatos, Th. C.; Christou, A. G.; Jones, C. M.; O'Callaghan, B. J.; Abboud, K. A.; O'Brien, T. A.; Christou, G. *J. Am. Chem. Soc.* **2007**, *129*, 9840. (b) Cañada-Vilalta, C.; O'Brien, T. A.; Brechin, E. K.; Pink, M.; Davidson, E. R.; Christou, G. *Inorg. Chem.* **2004**, *43*, 5505.

Table 4. Calculated Exchange Interactions (J_{AB}) and Spin Couplings ($\langle \hat{S}_A \cdot \hat{S}_B \rangle$) for **1** and **2**

complex	A	B	$J^{a,b}$	type [c]	$\langle \hat{S}_A \cdot \hat{S}_B \rangle$ [d]
1	1	2	+5.6	$Mn^{2+}Mn^{3+}$ ($J_{23(o)}$)	+5.02
	1	3	+5.9	$Mn^{2+}Mn^{3+}$ ($J_{23(o)}$)	+5.02
	2	5	+5.2	$Mn^{2+}Mn^{3+}$ ($J_{23(o)}$)	+5.04
	3	6	+6.6	$Mn^{2+}Mn^{3+}$ ($J_{23(o)}$)	+5.04
	5	7	+6.9	$Mn^{2+}Mn^{3+}$ ($J_{23(o)}$)	+5.04
	6	7	+6.0	$Mn^{2+}Mn^{3+}$ ($J_{23(o)}$)	+5.04
	4	1	+0.9	$Mn^{2+}Mn^{3+}$ ($J_{23(i)}$)	−5.25 [e]
	4	2	−0.9	$Mn^{2+}Mn^{2+}$ ($J_{22(i)}$)	−6.82
	4	5	+0.6	$Mn^{2+}Mn^{3+}$ ($J_{23(i)}$)	−5.51 [e]
	4	7	−0.9	$Mn^{2+}Mn^{2+}$ ($J_{22(i)}$)	−6.91
	4	6	+0.5	$Mn^{2+}Mn^{3+}$ ($J_{23(i)}$)	−5.50 [e]
	4	3	−0.8	$Mn^{2+}Mn^{2+}$ ($J_{22(i)}$)	−6.76
2	1	2	+7.6	$Mn^{2+}Mn^{3+}$ ($J_{23(o)}$)	+5.00
	1	2″	+5.0	$Mn^{2+}Mn^{3+}$ ($J_{23(o)}$)	+5.00
	3	1	+1.0	$Mn^{2+}Mn^{3+}$ ($J_{23(i)}$)	+5.00
	3	2	−0.6	$Mn^{2+}Mn^{2+}$ ($J_{22(i)}$)	+6.25 [e]

[a] cm^{-1}. [b] $\hat{\mathcal{H}} = -2 J_{AB} \hat{S}_A \cdot \hat{S}_B$ convention. [c] o = outer, *i* = inner; the subscripts on *J* refer to the Mn oxidation states—do not confuse with the atom labels of columns 2 and 3. [d] Positive and negative signs indicate parallel and antiparallel spin alignment, respectively. [e] Frustrated interactions.

parallel, the spin couplings from eq 8 are +6.25 and +5.00, respectively. The spin couplings for the outer $J_{23(o)}$ interactions in Table 4 are all +5.0, confirming parallel alignment of the outer spins. Similarly, for perfectly antiparallel alignment of a Mn^{2+}/Mn^{2+} or Mn^{2+}/Mn^{3+} pair, the spin couplings from eq 8 are −8.75 and −7.00, respectively. The calculated $J_{22(i)}$ (Mn^{2+}/Mn^{2+}) interactions in Table 4 are negative (antiferromagnetic) with spin couplings of ∼ −6.9, as expected (for antiparallel alignments, the calculated spin couplings are typically smaller than given by eq 8 because the perfectly antiparallel alignment is the main, but nevertheless not the only component of the spin wave function). However, the $J_{23(i)}$ (Mn^{2+}/Mn^{3+}) interactions of the Mn4Mn1, Mn4Mn5, and Mn4Mn6 pairs in Table 4 are ferromagnetic, and yet their spin couplings are very negative (∼ −5.3 to −5.5), that is, these ferromagnetic interactions are completely frustrated, and the spins are aligned antiparallel.

The origin of the $S = 11$ ground state is thus simpler than we had anticipated: as suspected, it is a spin frustrated system, but with (relatively) strong ferromagnetic coupling in the outer hexagon fixing the spin of this unit at $S = 27/2$; the overall molecular *S* is thus determined by one factor, the relative magnitude of the weaker $J_{22(i)}$ and $J_{23(i)}$ interactions. Note that this explanation is significantly different from that offered previously[51] to explain the origin of the $S = 11$ ground state in this Mn_7 family; this assumed that all interactions between the outer and inner Mn atoms were identical, that is, $J_{22(i)} = J_{23(i)}$. We did not feel that this approximation was a safe one, and this has been borne out by the present DFT calculations, which reveal that the $J_{22(i)}$ and $J_{23(i)}$ difference is in fact crucial to the observed ground state. We can thus rationalize the repeated observation of an $S = 11$ ground state in now five compounds as due to a strong $J_{23(o)}$ and the slightly stronger $J_{22(i)}$ versus $J_{23(i)}$ interactions, giving a simple spin-up/spin-down situation.

The above analysis reveals these Mn_7 molecules to be an interesting case where the ground state is determined

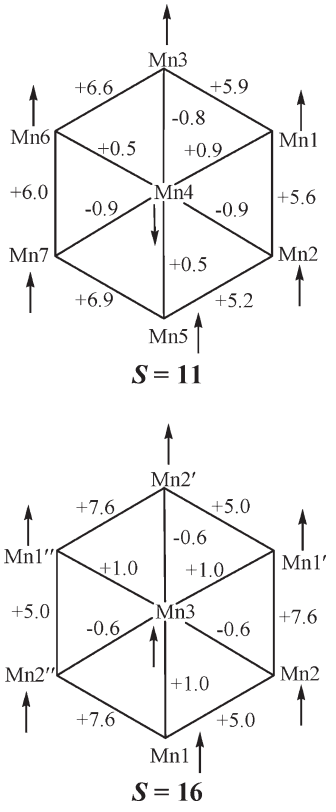

Figure 7. Calculated *J* values obtained by DFT for the anions of **1** (top) and **2** (bottom), using the $\hat{\mathcal{H}} = -2J_{AB}\hat{S}_A \cdot \hat{S}_B$ convention, and the resulting ground state spin alignments. The atom labels are those of Figure 1 (top and middle, respectively).

by the relative magnitude of the two weakest interactions. But, as such, they should be the most susceptible to significant change from structural perturbation, and this raised the question of whether it might be possible to maximize the spin ground state of these Mn_7 complexes by identifying the $S = 16$ variant resulting from parallel alignment of the inner spin with the outer hexagon. It was, in fact, for this reason that we have explored the synthesis of several related Mn_7 complexes in this work, seeking small changes to the ligand set and/or the cation, but trying to avoid major perturbation that would lead to a different type of reaction product. To cut a long story short, we have now identified $S = 16$ variants of the Mn_7 family for the first time, complexes **2** and **5**.

dc and ac Magnetic Susceptibility Studies on 2 and 5. Variable-temperature, solid-state magnetic susceptibility measurements were performed under the same conditions as for **1**, **3**, and **4**. For complex **2**·DMF, $\chi_M T$ continuously increases from 31.45 cm^3 K mol^{-1} at 300 K to 122.63 cm^3 K mol^{-1} at 5.0 K (Figure 4), clearly indicating a much larger ground state than for **1**, **3**, and **4**, and suggestive of an $S = 16$ ground state with $g \sim 1.9$ (the spin-only ($g = 2$) value is 136 cm^3 K mol^{-1}). $\chi_M T$ for **5** is very similar to **2**·DMF, continuously increasing from 30.83 cm^3 K mol^{-1} at 300 K to 120.23 cm^3 K mol^{-1} at 5.0 K (Supporting Information, Figure S7). To confirm the suggested $S = 16$ ground state, magnetization versus dc field data were collected as for **1** and **3** in magnetic fields (*H*) and temperatures of 1−50 kOe and 1.8−10.0 K, respectively. The resulting data are shown in Figure 8, and the near superimposition of the isofield lines indicates

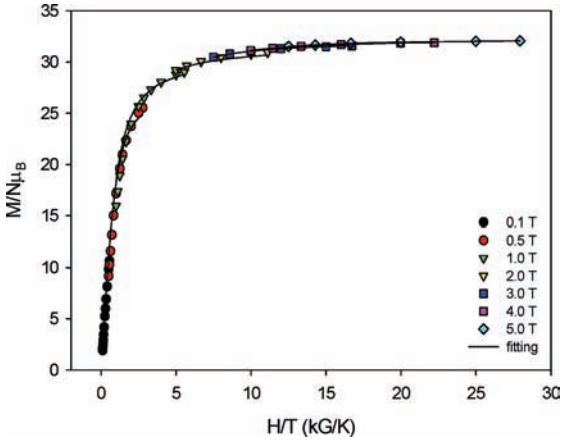

Figure 8. Plot of reduced magnetization ($M/N\,\mu_B$) vs H/T for complex **2**·DMF at applied fields of 0.1−5.0 T and in the 1.8−10 K temperature range. The solid lines are the fit of the data; see the text for the fit parameters.

little or no anisotropy. The data were fit using the program MAGNET,[23] and a good fit was obtained (solid lines in Figure 8) with $S = 16$, $g = 1.95$, and $D = -0.02$ cm^{-1}. Alternative fits with $S < 16$ were rejected because they gave unreasonably large values of g. The D value for **2**·DMF is noticeably smaller than those for **1** and **3**, which may seem surprising given that all three compounds have similar structures with similar disposition of the Mn^{III} JT elongation axes (O(2)−Mn(1)−N(4) for **2**·DMF). However, this is as expected from the fact that for a given type of compound, the D value is expected to decrease as the S value increases.[8,9]

The ac susceptibility studies, under the same conditions as for **1**, **3**, and **4**, confirmed an $S = 16$ ground state for **2**·DMF and **5**. The $\chi_M'T$ versus T plots in Figure 9 show $\chi_M'T$ to increase with decreasing temperature, and extrapolation from above 5 to 0 K gives $\chi_M'T$ of ∼ 125−135 cm^3 K mol^{-1}, confirming an $S = 16$ ground state with g slightly less than 2. Note that an $S = 16$ ground state is one of the largest observed to date.[10−14,59] Neither **2**·DMF (Supporting Information, Figure S8) nor **5** exhibited an ac out-of-phase (χ_M'') susceptibility signal down to 1.8 K, which is consistent with the fact that even though the spin has increased dramatically to $S = 16$, such that the barrier $U = S^2|D| = 256|D|$ for $S = 16$, the vanishingly small D value leads to an insignificant barrier of (at most) ∼5 cm^{-1}.

Theoretical Studies: Rationalization of the $S = 16$ Ground States of 2 and 5. Calculations were carried out on **2** using the same methods as above for **1**. The calculated energies and local Mn spin densities for each spin component are presented in Supporting Information, Table S3; as for **1**, the calculated spin densities were as expected and show that that correct spin distributions were obtained for all spin components considered. The exchange constants J_{AB} were obtained for **2** from the data of Supporting Information, Table S3, and they are listed together with the calculated spin couplings $\langle \hat{S}_A \cdot \hat{S}_B \rangle$ in Table 4. Once again, these results beautifully rationalize the experimental $S = 16$ ground state, yielding the

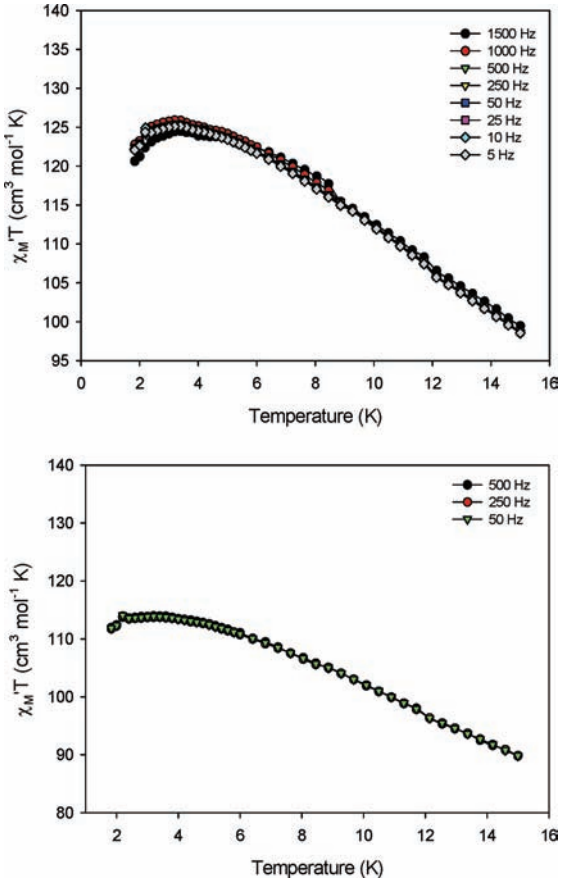

Figure 9. Plots of the ac in-phase $\chi'_M T$ vs T for complexes **2**·DMF (top) and **5** (bottom) at the indicated frequencies.

all-parallel spin alignments of Figure 7, bottom. The main and crucial difference with **1** is that the relative magnitude of $J_{22(i)}$ and $J_{23(i)}$ has reversed; the ferromagnetic $J_{23(i)}$ is now the stronger, frustrating $J_{22(i)}$ and aligning the central Mn^{2+} spin parallel to the outer hexagon to give an $S = {}^{27}/_2 + {}^{5}/_2 = 16$ ground state. The spin alignments of Figure 7 (bottom) are confirmed by the calculated spin couplings $\langle \hat{S}_A \cdot \hat{S}_B \rangle$ in Table 4. Again, the ferromagnetic $J_{23(o)}$ gives parallel alignment of all outer spins, as confirmed by the spin couplings of + 5.0. This time, however, the ferromagnetic $J_{23(i)}$ interactions of the Mn4Mn1, Mn4Mn5, and Mn4Mn6 pairs are slightly stronger than in **1**, and frustrate the slightly weaker antiferromagnetic $J_{22(i)}$ interactions. This is clear from the spin couplings: the ferromagnetic $J_{23(i)}$ interactions give +5.0 spin couplings, but the antiferromagnetic $J_{22(i)}$ interactions have positive spin couplings of +6.25, indicating parallel alignments. Thus, it is now the $J_{22(i)}$ interactions that are frustrated, and the central spin is parallel to the outer spins.

Structural Rationalization of the $S = 11$ to $S = 16$ Spin Switch. With $S = 16$ variants of the Mn_7 family attained, it is pertinent to ask whether any structural difference between them and the $S = 11$ complexes can be identified as the primary cause of the $J_{22(i)}$ versus $J_{23(i)}$ change and resulting ground state spin switch. Collected in Table 5 are the pertinent structural parameters of the [$Mn_7(\mu_3$-$O)_6(\mu$-$O)_6$] cores of **1**·MeOH and **2**·DMF·Et_2O averaged under C_{3v} core symmetry. It is difficult to identify any major change that can be considered beyond experimental uncertainties, which of course is consistent

(59) Tasiopoulos, A. J.; Wernsdorfer, W.; Moulton, B.; Zaworotko, M. J.; Christou, G. *J. Am. Chem. Soc.* **2003**, *125*, 15274.

Table 5. Core Metric Parameters (Å, deg) for **1**·MeOH and **2**·DMF·Et_2O

parameter[a]	**1**[b] (S = 11)	**2**[b] (S = 16)
$Mn^{II}_{(o)}\cdots Mn^{III}_{(o)}$	3.309	3.312
$Mn^{II}_{(o)}\cdots Mn^{II}_{(i)}$	3.305	3.324
$Mn^{III}_{(o)}\cdots Mn^{II}_{(i)}$	3.312	3.302
$Mn^{II}_{(o)}$–(μ-OR)	2.140	2.115
$Mn^{III}_{(o)}$–(μ-OR)	1.885	1.889
$Mn^{III}_{(o)}$–(μ-OR)	1.900	1.905
$Mn^{II}_{(o)}$–(μ_3-OR)	2.255	2.262
$Mn^{III}_{(o)}$–(μ_3-OR)	2.126	2.121
$Mn^{II}_{(i)}$–(μ_3-OR)	2.201	2.200
$Mn^{II}_{(o)}$–(μ-OR)–$Mn^{III}_{(o)}$	110.2	111.2
$Mn^{II}_{(o)}$–(μ_3-OR)–$Mn^{III}_{(o)}$	98.1	98.2
$Mn^{II}_{(i)}$–(μ_3-OR)–$Mn^{II}_{(o)}$	95.7	96.3
$Mn^{II}_{(i)}$–(μ_3-OR)–$Mn^{III}_{(o)}$	99.9	99.6

[a] o = outer, i = inner. [b] averaged under virtual C_{3v} core symmetry.

with the minimal changes in the calculated exchange parameters from DFT. The biggest difference is 1° found in the $Mn^{II}_{(o)}$–(μ-OR)–$Mn^{III}_{(o)}$ angle, but even this is statistically insignificant. Most relevant to the spin switch are the $Mn^{II}_{(i)}$–(μ_3-OR)–$Mn^{II}_{(o)}$ and $Mn^{II}_{(i)}$–(μ_3-OR)–$Mn^{III}_{(o)}$ angles, since these would be expected to influence $J_{22(i)}$ and $J_{23(i)}$. Although the averages are insignificantly different statistically, it is interesting that as one increases the other decreases in going from **1** to **2**, and vice versa, which parallels the change in $J_{22(i)}$ versus $J_{23(i)}$, and maybe this is providing an insight into the origin of the change in ground state. Nevertheless, we conclude that the core structures of **1** and **2** are indistinguishable within statistical uncertainties, and that very small changes indeed must be the origin of the change in ground state. It would not be an exaggeration to say that these complexes are essentially balanced on a knife-edge between S = 11 and 16, and it takes only small perturbations to push them one way or the other.

Magnetization Hysteresis Studies below 1.8 K. To complete our studies, we carried out micro-SQUID[24] measurements of magnetization versus dc field sweeps on single crystals of **1**·MeOH and **2**·DMF·Et_2O down to 0.04 K to explore whether either complex might exhibit a barrier indicative of a SMM. The obtained data for **1**·MeOH (Figure 10) show an interesting profile, with the saturated magnetization at either extremes relaxing considerably as the field is decreased below ~1 T. This is a signature of intermolecular antiferromagnetic interactions: a large applied field overcomes these and aligns all molecular spins parallel, but as the field is decreased to a weak enough value, the antiferromagnetic spin alignment of adjacent molecules begins to be re-established. This provides strong evidence supporting our assertion that significant intermolecular interactions through the Na^+ ion in **1**·MeOH were the cause of the complications experienced in the dc and ac magnetization studies and fits. Around zero field in Figure 10 is observed a hysteresis loop, which exhibits minimal scan rate dependence and only a small temperature dependence. This is not the behavior of SMMs, which display a marked increase in coercivity with increasing field sweep rate. We assign this hysteresis as being due to a barrier to relaxation that arises from a combination of the intermolecular interactions coupled with an intrinsic molecular anisotropy barrier. Unfortunately, we were unable to obtain the corresponding single-crystal data on complexes **3**·MeCN·Et_2O or **4** to remove the effect of the Na^+ ion.

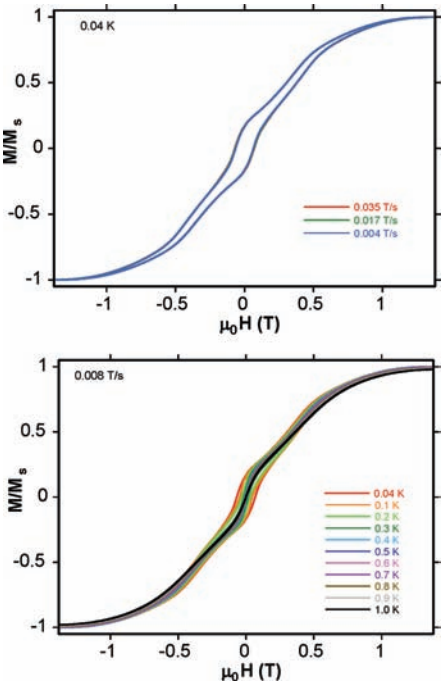

Figure 10. Magnetization vs applied dc field scans for a single-crystal of **1**·MeOH at the indicated field sweep rates (top) and temperatures (bottom). The magnetization is normalized to its saturation value, M_S.

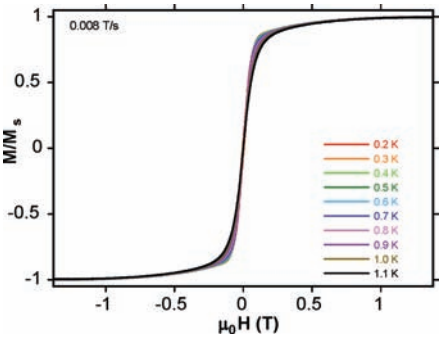

Figure 11. Magnetization vs applied dc field scans for a single-crystal of **2**·DMF·Et_2O at the indicated temperatures. The magnetization is normalized to its saturation value, M_S.

The data for S = 16 complex **2**·DMF·Et_2O are shown in Figure 11, and the scan profile shows no evidence of intermolecular interactions, nor of any hysteresis indicative of a barrier to magnetization relaxation. The first point is consistent with the different way adjacent molecules are connected via the Na^+ ion, as discussed earlier, and the finding that problems assignable to intermolecular interactions were not encountered in the dc and ac magnetization studies on **2**·DMF·Et_2O. The second point emphasizes again the importance of having both a large S and a significant anisotropy, D, to obtain a SMM.

Summary and Conclusions

The combination of N_3^- or Cl^- with the alcohol-containing $mdaH_2$ or $teaH_3$ has proved to be a useful route to mixed-valence Mn_7 disk-like complexes. Three of these, together with

the two previous examples in the literature, possess $S = 11$ ground states, and this has been rationalized as due to a (relatively) strongly ferromagnetically coupled outer Mn_6 hexagon with $S = {}^{27}/_{2}$ aligned antiparallel to a central Mn^{2+} ion. The fact that the ground state is determined by the relative magnitude of the two inner $J_{22(i)}$ and $J_{23(i)}$ interactions suggested it should be possible to increase the spin to its maximum of $S = 16$ by relatively small perturbations of the structure, and this has now been accomplished, as described. This "spin maximization" is, in fact, an extension of the "spin tweaking" studies that we have reported in recent years, in which small, ligand-induced structural perturbations of a spin-frustrated cluster with an already high ground state S value changes the relative magnitude of the competing exchange interactions and thus the observed ground state; for example, certain Mn_{25} clusters with $S = {}^{51}/_{2}$ can be converted to $S = {}^{61}/_{2}$ by modification of their ligation, but the maximum of $S = {}^{105}/_{2}$ was not reached.[8a,b] Similarly, a family of Mn_6 clusters has been made in which the ground state S can be varied over a range up to the maximum $S = 12$.[8c,d] The beauty of the present Mn_7 complexes is how the ground state can be increased by almost 50% as a function of a single property of the molecule, the $J_{22(i)}$ versus $J_{23(i)}$ relative magnitude, and thus the orientation of the single central Mn^{2+} spin.

We close with some comments about the DFT calculations: all the obtained values are very small, particularly $J_{22(i)}$ and $J_{23(i)}$, and it should be explicitly stated that within typical uncertainties it cannot be concluded from the DFT calculations on **1** and **2** per se whether $J_{22(i)}$ is bigger than $J_{23(i)}$, or vice versa. In other words, had we obtained the crystal structures of **1** and **2** and performed the DFT calculations, we would not have attempted to predict from the obtained results what the ground states of the two complexes were; the obtained J values are simply too similar, and it would have been completely unreliable to use them for predictive purposes. What we have done instead, once the $S = 11$ versus $S = 16$ difference had been experimentally established, is used the DFT calculations to gain insight into the origin of the difference. For this purpose, we feel the calculations are reliable, especially given the stronger outer interactions, as is the conclusion that the ground state is a consequence of the relative magnitude of the antiferromagnetic $J_{22(i)}$ versus the ferromagnetic $J_{23(i)}$ interactions. Further studies are in progress.

Acknowledgment. This work was supported by NSF Grants CHE-0414555 and CHE-0910472. The theoretical calculations were supported by an IBM Shared University Research grant to IU (T.O'B.). K.M.P. acknowledges funding from the Undergraduate Research Opportunities Program at IUPUI.

Supporting Information Available: Structural and magnetism figures, and X-ray crystallographic files in CIF format for complexes **1**·MeOH, **2**·DMF·Et_2O, and **3**·MeCN·Et_2O. This material is available free of charge via the Internet at http://pubs.acs.org.